Molecular Cell
Article

SIRT6 Recruits SNF2H to DNA Break Sites, Preventing Genomic Instability through Chromatin Remodeling

Debra Toiber,[1] Fabian Erdel,[2] Karim Bouazoune,[3] Dafne M. Silberman,[1,4] Lei Zhong,[1] Peter Mulligan,[1,5] Carlos Sebastian,[1] Claudia Cosentino,[1] Barbara Martinez-Pastor,[1] Sofia Giacosa,[1] Agustina D'Urso,[1,6] Anders M. Näär,[1,5] Robert Kingston,[3] Karsten Rippe,[2] and Raul Mostoslavsky[1,*]

[1]The Massachusetts General Hospital Cancer Center, Harvard Medical School, Boston, MA 02114, USA
[2]Research Group Genome Organization and Function, Deutsches Krebsforschungszentrum (DKFZ) and BioQuant, 69120 Heidelberg, Germany
[3]Department of Molecular Biology, Massachusetts General Hospital, and Department of Genetics, Harvard Medical School, Boston, MA 02115, USA
[4]Department of Human Biochemistry, Medical School, CEFyBO-UBA-CONICET, Buenos Aires C1121ABG, Argentina
[5]Department of Cell Biology, Harvard Medical School, Boston, MA 02115, USA
[6]Present address: Department of Molecular Biosciences, Northwestern University, Evanston, IL 60208, USA
*Correspondence: rmostoslavsky@mgh.harvard.edu
http://dx.doi.org/10.1016/j.molcel.2013.06.018

SUMMARY

DNA damage is linked to multiple human diseases, such as cancer, neurodegeneration, and aging. Little is known about the role of chromatin accessibility in DNA repair. Here, we find that the deacetylase sirtuin 6 (SIRT6) is one of the earliest factors recruited to double-strand breaks (DSBs). SIRT6 recruits the chromatin remodeler SNF2H to DSBs and focally deacetylates histone H3K56. Lack of SIRT6 and SNF2H impairs chromatin remodeling, increasing sensitivity to genotoxic damage and recruitment of downstream factors such as 53BP1 and breast cancer 1 (BRCA1). Remarkably, SIRT6-deficient mice exhibit lower levels of chromatin-associated SNF2H in specific tissues, a phenotype accompanied by DNA damage. We demonstrate that SIRT6 is critical for recruitment of a chromatin remodeler as an early step in the DNA damage response, indicating that proper unfolding of chromatin plays a rate-limiting role. We present a unique crosstalk between a histone modifier and a chromatin remodeler, regulating a coordinated response to prevent DNA damage.

INTRODUCTION

Preservation of DNA integrity is critical to ensure accurate inheritance of the genetic material, as well as proper cellular and organismal function. Intrinsic and extrinsic processes, such as DNA transcription and replication, cellular metabolism, and environmental challenges, represent persistent genotoxic threats. Indeed, unrepaired DNA damage can frequently lead to cell senescence, apoptosis, or tumorigenesis and thus jeopardize organismal well-being (Papamichos-Chronakis and Peterson, 2013). Multiple mechanisms have thus evolved to protect and repair damaged DNA. Probably the most critical DNA lesions are double-strand breaks (DSBs), which can result in loss of genetic material, mutations, and deleterious translocations. Consequently, cells have evolved two primary DSB repair mechanisms: nonhomologous end-joining (NHEJ), a mutation-prone pathway that repairs DSBs by joining two ends together, and the error-free homologous recombination (HR) pathway, which operates only when sister chromatids are paired together (Chapman et al., 2012). A number of factors are involved in the recognition, amplification, and repair cascade that is triggered by DSBs, a process known as the DNA damage response (DDR) (Ciccia and Elledge, 2010). In this orchestrated response that is set in motion, breaks are sensed by members of the poly(ADP-ribose) polymerase (PARP) family, which activates phosphoinositide 3-kinase (PI3K)-related kinases including ataxia telangiectasia mutated (ATM), ataxia telangiectasia and Rad3-related protein (ATR), and DNA-dependent protein kinase (DNA-PK). These proteins in turn recruit sensors that amplify the signal, including the MRN (MRE11-RAD50-NBS1) complex and multiple histone modifiers (such as Tip60, RING finger protein 8 (RNF8), and RNF168), which orchestrate a broad spectrum of histone posttranslational modifications, including methylation, acetylation, ubiquitylation, and phosphorylation. In turn, these modifications work in concert to recruit DNA repair factors, such as 53BP1, Rad51, and DNA ligases to faithfully repair the broken DNA (Lukas et al., 2011).

Eukaryotic DNA is packaged within nucleosomes, which represents an additional physical barrier for DDR factors to access damaged DNA. Only in recent years has the role of chromatin accessibility in DNA repair begun to emerge. Various chromatin remodelers, including INO80 (Gospodinov et al., 2011; Kashiwaba et al., 2010; Neumann et al., 2012; Papamichos-Chronakis et al., 2011), SMARCAD1 (Fun 30 in yeast) (Chen et al., 2012; Costelloe et al., 2012; Lee et al., 2010), p400 (Xu et al., 2010, 2012), chromodomain helicase DNA-binding protein 4 (CHD4) (Larsen et al., 2010; Polo et al., 2010), and the nucleosome

remodeling and histone deacetylase (NuRD) complex (Smeenk et al., 2010), were shown to be recruited to damage sites, suggesting the need of chromatin relaxation and remodeling in order to allow repair (Papamichos-Chronakis and Peterson, 2013). Notably, most of the above factors have been mainly characterized in yeast, and whether mammalian cells exhibit alterations in chromatin structure during DSB repair as well as the precise mechanisms regulating chromatin dynamics in the context of DNA repair remain poorly understood. Interestingly, the imitation switch (ISWI) family member SNF2H, an ATP-dependent chromatin remodeler with roles in transcription and replication (Erdel and Rippe, 2011), has been proposed to be recruited to DNA damage sites downstream of the ubiquitin ligase RNF20 (Erdel et al., 2010; Lan et al., 2010; Nakamura et al., 2011; Smeenk et al., 2010). However, the specific signals recognized by SNF2H for its targeting to DNA damage sites remain unknown.

In this study, we have uncovered a unique role for the histone deacetylase sirtuin 6 (SIRT6) as a scaffold protein in DDR. SIRT6 is a chromatin-bound protein that belongs to the highly conserved sirtuin family of NAD(+)-dependent deacetylases, with various roles in DNA damage, metabolism, and cancer (Finkel et al., 2009; Mostoslavsky et al., 2006; Toiber et al., 2011; Zhong et al., 2010). Following DNA damage, SIRT6 is recruited to DSB sites within seconds, specifically recruiting the chromatin remodeler SNF2H to open up condensed chromatin and deacetylating H3K56, both critical steps required for proper recruitment of downstream DDR factors and efficient DNA repair.

RESULTS

SIRT6 Interacts with the Chromatin Remodeler SNF2H

In previous studies, we have shown that SIRT6-deficient cells accumulate genomic instability (Mostoslavsky et al., 2006), yet the precise molecular mechanism behind this defect remained unclear. In order to gain further insights into the molecular functions of SIRT6, we employed affinity purification to identify associated proteins. Flag-tagged SIRT6 was expressed in human embryonic kidney (HEK) 293T cells and used as a bait to identify interacting proteins by mass spectrometry. One of the top five most abundant SIRT6-interacting proteins was the ISWI family member SNF2H (Figure 1A; see also Supplemental Experimental Procedures). We first confirmed this interaction by reciprocal immunoprecipitation (IP) following Flag-SIRT6 expression in 293T cells (Figure 1B), which demonstrates a clear interaction between these proteins. To determine whether such interaction is physiologically relevant, we performed reciprocal coimmunoprecipitation (coIP) assays with endogenous proteins. Figure 1C shows that endogenous SIRT6 associated with SNF2H in mouse embryonic stem cells (ESCs), indicating that these two proteins interact under physiological conditions. To interrogate the specific domains in SIRT6 that were required for this interaction, we expressed SIRT6 lacking the amino terminus (N), carboxyl terminus (C), or both domains (Tennen et al., 2010). As shown in Figure 1D, lack of the C terminus completely abolished the interaction, indicating that this domain was necessary for SNF2H binding. To further confirm whether SIRT6 interacts directly with SNF2H, we generated bacterial recombinant, purified glutathione S-transferase (GST)-SIRT6 proteins encompassing the full-length protein (334 amino acids), the C terminus, the catalytic core, or the N terminus of SIRT6 and measured interaction with purified recombinant SNF2H. In vitro binding assays indicated that GST-SIRT6 interacts directly with SNF2H and confirmed that SNF2H binds preferentially to the C terminus of SIRT6 (Figures 1E and S1 available online). Notably, SIRT6 also interacted with multiple proteins described earlier as SNF2H partners (Figure S2A), including ACF1 and WSTF, two additional subunits of SNF2H-containing chromatin remodeling complexes (Figures S2A and S2B), indicating that SIRT6 may associate with one of these complexes. Indeed, glycerol gradient fractionation clearly showed that SNF2H and SIRT6 copurified in the same molecular weight (MW) fractions (fractions 7–9, 11, and 12, Figure 1F). Notably, SNF2H was absent in the higher MW fractions of SIRT6-deficient samples (fractions 7–9, Figure 1G), indicating that SIRT6 is required for the association of SNF2H into these higher-molecular-weight complexes.

SIRT6 Enhances SNF2H Nucleosome Binding

Given the interaction of SIRT6 and SNF2H, we evaluated whether SIRT6 may modulate SNF2H activity and nucleosome binding in vitro. We first measured SNF2H remodeling activity through the restriction enzyme accessibility assay. No differences in SNF2H-dependent chromatin remodeling were observed in the presence or absence of SIRT6 (data not shown), indicating that SIRT6 does not modulate SNF2H remodeling activity. We then tested whether SIRT6 may modulate SNF2H nucleosome binding in vitro. First, we found that SIRT6 binds to nucleosomes even at nM concentrations, and when added together, SIRT6 and SNF2H are able to bind to the same nucleosome, resulting in a different nucleosome shift compared to the shift observed with the individual enzymes. Importantly, in the presence of SIRT6, SNF2H bound nucleosomes at lower concentrations than when incubated alone (Figure 1H). When we quantified levels of free nucleosomes and nucleosomes bound under the different conditions (Figure S1B), SIRT6 reduced the levels of free nucleosomes in the presence of SNF2H by at least 2-fold, indicating that, even in vitro, the presence of SIRT6 increased the ability of SNF2H to bind nucleosomes.

SIRT6 Recruits SNF2H to Chromatin

Given the disappearance of SNF2H from the glycerol gradient heavy fractions in SIRT6-deficient cells, we first evaluated whether SIRT6 could modulate SNF2H stability or expression. We did not observe any difference in total SNF2H protein levels in whole-cell extracts (WCEs) from SIRT6-deficient mouse ESCs (Figure 2A). Thus, SIRT6 does not affect total SNF2H protein levels. Given their tighter interaction with nucleosomes (Figure 1H), a second possibility would be that SIRT6 and SNF2H interact specifically on chromatin, and lack of SIRT6 might affect chromatin binding of SNF2H. Indeed, biochemical fractionation assays revealed a striking reduction of SNF2H in SIRT6-deficient chromatin fractions (Figure 2A). In order to validate these results, we silenced SIRT6 in two other cell types, U2OS and 293T cells. Again, SNF2H was significantly reduced in chromatin following SIRT6 RNAi-mediated knockdown (KD) in these cells (Figures S2D and S2E). In addition, we took advantage of a catalytic

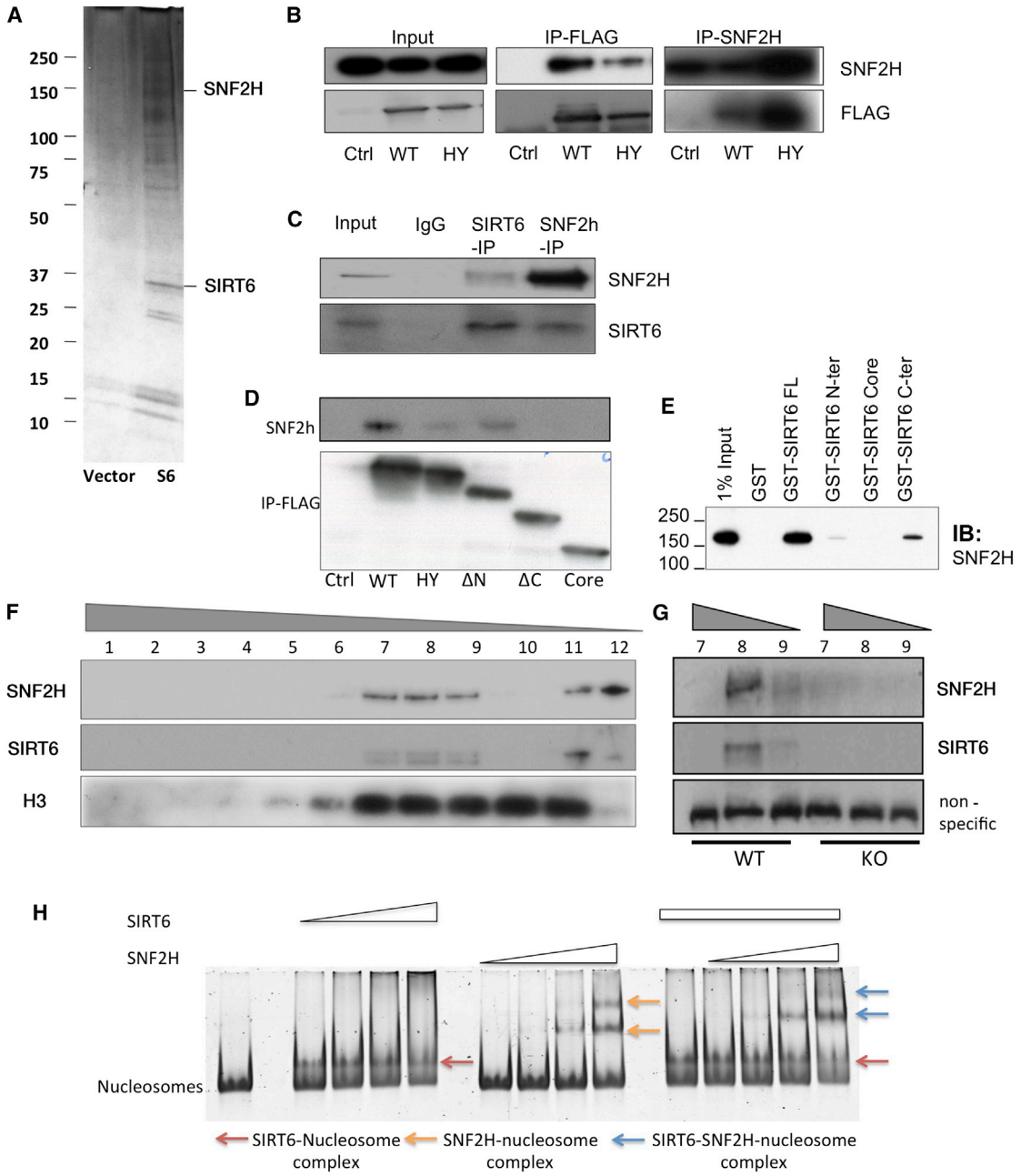

Figure 1. SIRT6 Interacts with SNF2H and Recruits It to Chromatin

(A) Flag-IP of protein extracts from Flag-SIRT6- or empty vector-expressing cells were used for mass spectrometry analysis where SNF2H was identified as a SIRT6 interactor. Silver-staining of extracts from Flag-control (Vector) or SIRT6-Flag-transfected cells is shown.

(B and C) Exogenous (B) and endogenous (C) coIPs were performed, and western blots were developed with the indicated antibodies. Flag-vector (Ctrl)-, Flag-WT-SIRT6 (WT)-, and Flag-HY-SIRT6 (HY)-transfected cells.

(D) IP for SIRT6-Flag (WT), SIRT6-HY (HY), and SIRT6 fragments lacking N (ΔN), C (ΔC), or both termini (Core).

(E) GST-full-length SIRT6 and SIRT6 C terminus, N terminus, or core domain were tested in vitro for interaction with baculovirus-purified SNF2H.

(F) Glycerol gradient fractionation for WT cells showing SIRT6, SNF2H, and H3 bands.

(G) Fractions 7–9 from WT and 7–9 from SIRT6 KO cells.

(H) Nucleosome shift assay was performed with 75 nM nucleosomes, SIRT6 (μM range), and SNF2H (nM range). The different complexes formed with the nucleosomes under SIRT6 and SNF2H incubation, or both proteins, are marked with the arrows. See also Figure S1.

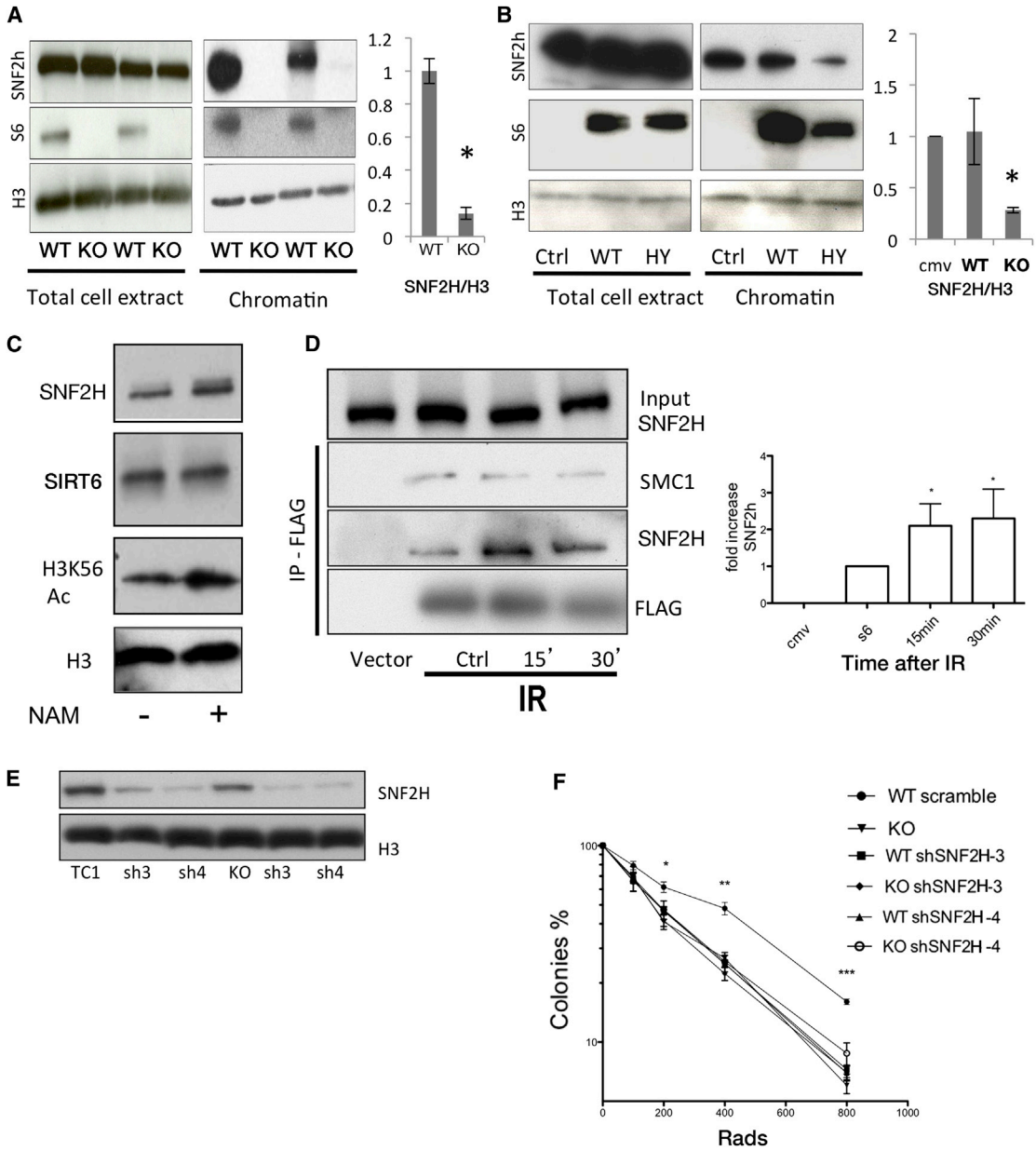

Figure 2. SIRT6 and SNF2H Act Together in DNA Repair

(A) Whole-cell extracts (WCEs) and chromatin fractions from WT and SIRT6 KO cells, showing impaired SNF2H recruitment to chromatin. Quantification of SNF2H levels within the chromatin fraction in three independent experiments is shown.

(B) SIRT6-WT and SIRT6-HY mutants were expressed in 293T cells, and the presence of SNF2H in WCEs and chromatin was analyzed by western blot. Quantification of SNF2H levels within the chromatin fraction in three independent experiments is shown.

(C) Western blot with the indicated antibodies was performed using chromatin fractions of NAM-treated or untreated cells.

(D) Cells were irradiated, and Flag-SIRT6 was immunoprecipitated 15 or 30 min after IR exposure. Cohesin protein SMC1 is shown as a SIRT6 interactor that was not affected by damage as a control.

(E) SNF2H expression was silenced in *Sirt6*$^{+/+}$ and *Sirt6*$^{-/-}$ ESCs using two different shRNA sequences.

(F) Survival assays upon IR of ESCs of the indicated genotypes. Data are represented as mean ± SEM (right panel, *$p < 0.01$, **$p < 0.001$, ***$p < 0.0001$). See also Figure S2.

domain mutant form of SIRT6, SIRT6-HY, which remains mainly in the cytoplasm but still interacts with SNF2H. When SIRT6-HY was overexpressed, SNF2H was significantly decreased in the chromatin fraction, further supporting the conclusion that SIRT6 is required to recruit SNF2H to chromatin (Figure 2B). Finally, we tested whether inhibition of the catalytic activity of chromatin-bound SIRT6 could impair SNF2H recruitment. For this purpose, we treated wild-type (WT) cells with nicotinamide

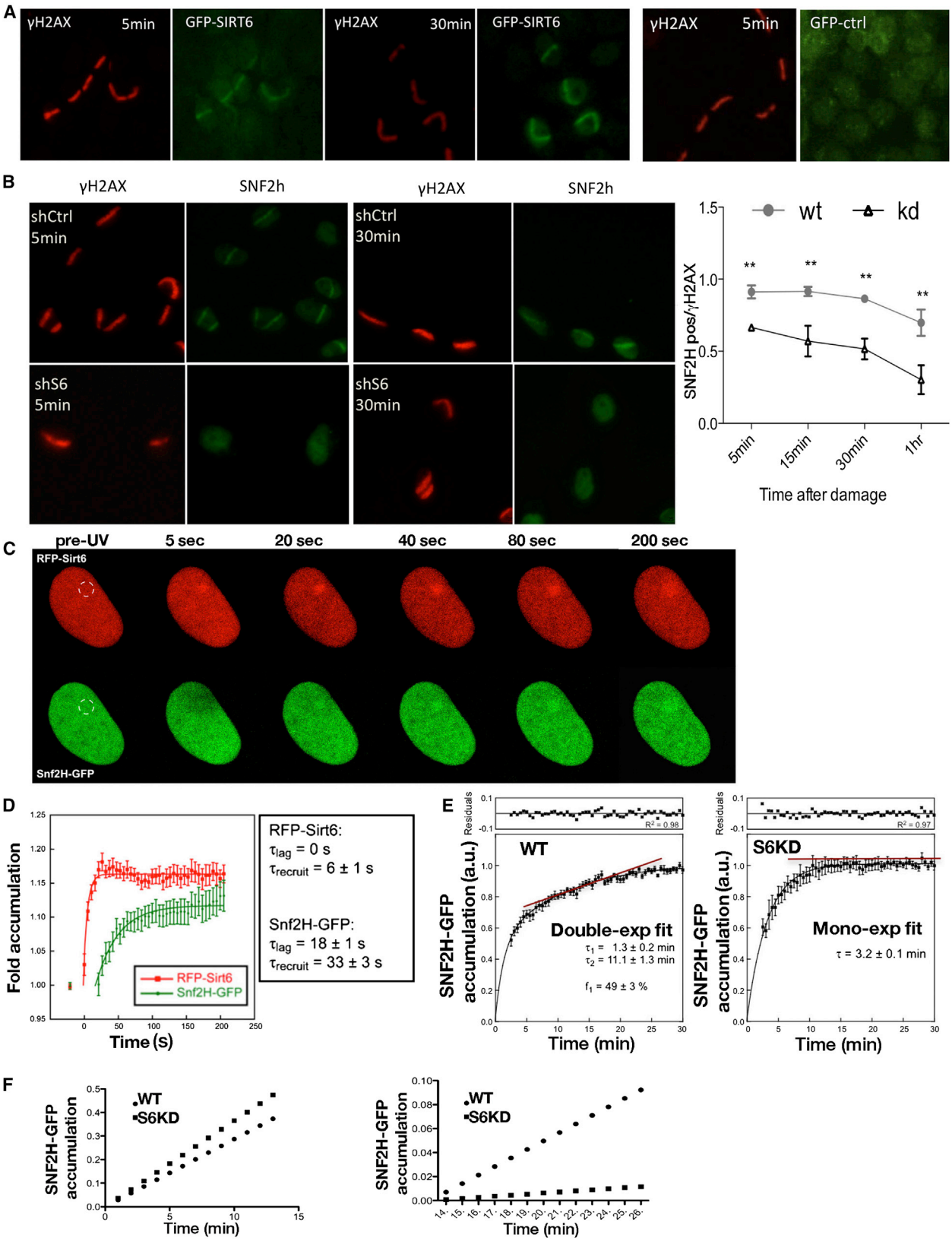

(legend on next page)

(NAM), a sirtuin inhibitor. Inhibition of SIRT6 was confirmed, as H3K56 acetylation (a SIRT6 substrate) was clearly elevated. However, SNF2H recruitment to chromatin was unaffected (Figure 2C), indicating that SIRT6 catalytic activity and H3K56 acetylation are not required for SNF2H recruitment when SIRT6 is already present on chromatin. Together, the above studies clearly demonstrate that SIRT6 is required both in vitro and in mammalian cells to recruit and maintain SNF2H on chromatin.

SIRT6 and SNF2H Act as Epistatic Genes

Previous studies have indicated that SNF2H may play a role in promoting genome integrity (Lan et al., 2010). Interestingly, we found that the interaction between SIRT6 and SNF2H increased rapidly upon ionizing radiation (IR) treatment (Figure 2D), suggesting that SIRT6 may recruit SNF2H to DNA damage sites. To test whether these proteins may act in concert to maintain proper DNA repair, we silenced SNF2H in both WT and SIRT6-deficient ESCs (Figure 2E) and measured survival rates in clonogenic assays. As we showed previously (Mostoslavsky et al., 2006), SIRT6-deficient cells exhibited hypersensitivity to IR. The same phenotype was observed in WT cells in which SNF2H was silenced. However, when SNF2H was silenced in SIRT6-deficient cells, there was no additive effect on survival (Figure 2F). In this context, SIRT6-deficient cells exhibited increased basal levels of phosphorylated p53, a marker of DNA damage checkpoint activation. SNF2H silencing in these cells did not cause any further increase in p53 phosphorylation, whereas SNF2H silencing in WT cells caused elevated p53 phosphorylation (Figure S2F). Together with the repair assays discussed below, these results indicate that SIRT6 and SNF2H may work through a common pathway.

SIRT6 Recruits SNF2H to the DNA Damage Sites

Several lines of evidence suggest that SNF2H might be recruited specifically to DSBs through its interaction with SIRT6: (i) both SIRT6 and SNF2H are chromatin-bound proteins, and SIRT6 enhanced SNF2H binding to chromatin under basal conditions (Figures 1H and 2A–2D); (ii) SIRT6 is mobilized to DNA damage sites (Kaidi et al., 2010; McCord et al., 2009); and (iii) interaction between SIRT6 and SNF2H was enhanced upon IR (Figure 2D). To further explore this possibility, we measured the recruitment kinetics of SNF2H to DNA break sites, taking advantage of a laser-induced DNA break assay. Specifically, we scored for cells with staining for both the DSB marker γH2AX and SNF2H and measured which proportion of γH2AX-stained cells exhibited SNF2H staining. Notably, SNF2H readily accumulated at DNA damage sites within 5 min in control cells, while such recruitment in SIRT6 downregulated (shSIRT6) cells was less efficient and clearly diminished over time (Figure 3B), pointing to a defect in recruitment and/or stabilization of SNF2H at DNA damage sites.

To further characterize SIRT6 and SNF2H kinetics upon DNA damage in real time, we took advantage of a red fluorescent protein (RFP)-SIRT6/SNF2H-green fluorescent protein (GFP) system analyzed with live-cell microscopy. Consistent with previous publications (Kaidi et al., 2010; McCord et al., 2009), we observed recruitment of SIRT6 to DNA breaks, but with much faster kinetics than previously reported, arriving at breaks 5 s after DNA damage and reaching a plateau after 30 s. This finding places SIRT6 within the fastest enzymes recruited to DNA damage sites (Figures 3C and 3D). SNF2H mobilization to DNA damage sites, although rapid, occurred after SIRT6 recruitment (Figures 3C and 3D). The time course plot shows that the time constant for reaching 50% of the plateau value is ~40 s lower for SIRT6 with respect to SNF2H, indicating a recruitment rate ~5 times faster for RFP-SIRT6 than for SNF2H-GFP. As noted, RFP-SIRT6 recruitment starts earlier after damage induction than that of SNF2H-GFP, consistent with SIRT6 bringing SNF2H to break sites.

SIRT6 Accelerates SNF2H Binding to DSBs

Our results suggest that SIRT6 brings SNF2H to damage sites. In order to further dissect this process, we generated shSIRT6 or scramble shRNA control (shCtrl) cell lines stably expressing a SNF2H-GFP protein (Figures 3E and S3A) (Erdel et al., 2010). In this system, we measured SNF2H-GFP recruitment to damage sites induced by bromodeoxyuridine (BrdU) presensitization and UV laser irradiation (a treatment that primarily generates DSBs). While shCtrl cells exhibited a clear biphasic SNF2H recruitment (i.e., rapid recruitment within seconds, followed by a slower phase of accumulation starting around 7 min), shSIRT6 cells were monophasic, presenting only the early SNF2H recruitment phase (Figures 3C and 3D). These results indicate that the second phase of SNF2H recruitment is dependent on SIRT6 (Figures 3C and 3D). To distinguish between active recruitment and stabilization of SNF2H by SIRT6, we used fluorescence loss in photobleaching (FLIP) experiments, in which the decay of SNF2H-GFP signal was measured during both early and late phases, and fluorescence recovery after photobleaching (FRAP) experiments, in which damage sites were bleached and the SNF2H-GFP recovery was measured. In these assays, the decay and the recovery of SNF2H-GFP were identical in shCtrl and shSIRT6 U2OS cells at both time points (early and late)

Figure 3. Kinetics of SIRT6 and SNF2H Recruitment to DSBs

(A) Laser-induced DNA damage was performed in cells transfected with GFP or GFP-SIRT6, fixed at indicated time points, and immunostained with anti-γH2AX and anti-GFP antibodies.

(B) Laser-induced DNA damage was performed in U2OS shCtrl or shSIRT6 cells immunostained with γH2AX and SNF2H at different time points. Graph shows time course analysis. SNF2H-positive cells among γH2AX-positive cells were quantified.

(C) RFP-SIRT6 and SNF2H-GFP recruitment was measured on damage sites and followed over time with live-cell imaging. A representative series is shown.

(D) Quantitative analysis of the recruitment experiments described in (C).

(E) Analysis of SNF2H recruitment in shCtrl versus shSIRT6 cells. Fluorescence intensity is normalized as 1 = maximum intensity reached in each case after 30 min.

(F) Graphic representation of the early- and late-recruitment phases of the graphs shown in (E). Data are represented as mean ± SEM. *$p < 0.05$, **$p < 0.001$. See also Figure S3.

(Figure S4B), indicating that stability of SNF2H binding is independent of SIRT6. Interestingly, our FLIP and FRAP results revealed that SNF2H turnover during the early accumulation phase was fast, indicating labile SNF2H binding at the site of breaks in this phase. On the contrary, during the late accumulation phase, SNF2H-GFP remained bound at DNA damage sites for a longer period of time. Since no differences in the SNF2H dissociation kinetics were observed between shCtrl and shSIRT6 cells, we concluded that SIRT6 does not stabilize chromatin-bound SNF2H (i.e., it does not reduce its kinetics dissociation rate), but rather accelerates SNF2H association to damage sites.

To evaluate whether the SIRT6-independent recruitment (rapid and unstable) of SNF2H occurs at double-strand breaks or at other types of DNA lesions, we used nonpresensitized cells (UV irradiation only). This UV treatment causes mainly pyrimidine dimers, abasic sites, and single-strand breaks (resembling oxidative damage) (Kielbassa et al., 1997; Pierce et al., 2001). In this experiment, both shCtrl and shSIRT6 cells exhibited the early SNF2H recruitment phase (Figure S4C), while the late SNF2H recruitment phase was absent, and this unstable SNF2H signal decayed early in both cell types (Figure S4D). Overall, these results strongly suggest that DNA single-strand breaks and other non-DSB lesions cause a brief and unstable SNF2H recruitment that is independent of SIRT6. On the other hand, stable SNF2H recruitment, specific to DSBs, occurs in a SIRT6-dependent fashion.

SIRT6 and SNF2H Are Required for Efficient DNA Repair

To confirm that SIRT6-dependent SNF2H recruitment is essential for DSB repair, we took advantage of U2OS cells that were engineered to induce a unique DNA cut upon expression of the I-SceI endonuclease (Pierce et al., 2001) (Figure 4A). First, we measured SIRT6 recruitment to damage sites, confirming its enrichment after DSB induction (Figure 4B). Second, we stably knocked down SIRT6 in these cells and performed chromatin immunoprecipitation (ChIP) of SNF2H to analyze its enrichment at the DNA break site using specific primers. In shCtrl cells, SNF2H was clearly recruited to the I-SceI break (Figure 4B). Strikingly, SNF2H recruitment was completely abolished in SIRT6 knockdown cells (Figure 4B). In order to confirm that SIRT6 is required to bring SNF2H to break sites, we performed a sequential ChIP-reChIP assay following I-SceI induction. In this assay, the SIRT6-chipped chromatin exhibited more than ~25-fold enrichment for SNF2H binding following induction of the break (Figure 4B). These studies are consistent with our immunofluorescence and live-imaging results and further demonstrate that SIRT6 is necessary for SNF2H recruitment to specific DSBs.

Additionally, the I-SceI system allowed us to analyze HR efficiency (Figure 4A). In these cells, a truncated GFP is restored to its functional form when DSBs are repaired. A fraction of ~4%–7% of control cells was GFP positive after induction of DNA breaks, while in the absence of SIRT6 such repair activity was completely lost (Figure 4C). Similar results were observed when SIRT6 activity was inhibited by nicotinamide (NAM) (Figure 4D). Re-expression of WT SIRT6 in shSIRT6 cells rescued the repair phenotype, whereas neither the SIRT6-HY nor the SIRT6-ΔC (catalytically active but unable to bind SNF2H) rescued the defects in DNA repair (Figure 4E). Overall, these results indicate that both SIRT6-dependent SNF2H recruitment and SIRT6 catalytic activity are necessary for DNA repair.

To further investigate the roles of SIRT6 and SNF2H in DNA repair, we used a transient direct repeat (DR)-GFP/I-SceI system in which both HR and NHEJ could be tested following the silencing of SIRT6, SNF2H, or both. As previously shown, shSIRT6 completely abolished HR, and similar results were observed in the shSNF2H or double knockdown cells (Figures S4A and S4B). Notably, we also observed a significant defect in NHEJ repair (Figure S4C), indicating that chromatin remodeling is required for both HR and NHEJ pathways.

Chromatin Relaxation Is Necessary for Proper DSB Repair

Previous studies have shown that defects in DNA damage repair in SNF2H knockdown cells could be rescued with chloroquine treatment, a drug that causes chromatin relaxation (Murr et al., 2006; Nakamura et al., 2011). Strikingly, DNA damage repair was fully rescued when we treated shSIRT6 cells with chloroquine (Figure 4F), suggesting that SIRT6 and SNF2H open chromatin at DNA damage sites, and opening of chromatin by chemical means was sufficient to bypass the requirement for either SIRT6 or SNF2H.

We predicted that SIRT6-dependent SNF2H recruitment was required in order to catalyze nucleosome remodeling; therefore, chromatin would remain compacted at DSBs in the absence of SIRT6. To test this hypothesis, we developed an assay using a similar system to the I-SceI system described above. Following I-SceI induction, DNA was digested with micrococcal nuclease (MNase), and the digested DNA was resolved on an agarose gel to separate nucleosomal fragments (Figure 4G). Enrichment for DSBs was measured by quantitative PCR (qPCR) near the damage site using specific primers. shCtrl cells exhibited a clear increase in chromatin relaxation following DNA damage, as reflected by the enrichment of the I-SceI locus in the mononucleosome fraction and its concomitant depletion from dinucleosomes (Figure 4H). In contrast, the amount of DSBs in mononucleosomes did not increase in shSIRT6 cells upon DNA damage, indicating that the chromatin flanking the breaks remained less accessible to MNase digestion following DNA damage in these cells (Figure 4H). No difference was observed when we measured accessibility at a downstream region located 2 kb from the I-SceI site (Figure S4D), indicating that the opening of chromatin occurs only locally at the DSB site. Consistent with these results, radial expansion of SNF2H at the damage sites was moderate and did not change in SIRT6-deficient cells (Figure S4F). As in our previous experiment, chloroquine treatment rescued the chromatin relaxation defect in SIRT6 knockdown cells (Figure S4E), further confirming our conclusion that increased local chromatin accessibility is required for proper DNA repair.

SIRT6 Deacetylates Histone H3K56 at DNA Damage Sites

SIRT6 is known to function as a histone H3K56 deacetylase (Michishita et al., 2009; Yang et al., 2009). In addition, previous studies have indicated that H3K56 is actively deacetylated at DNA break

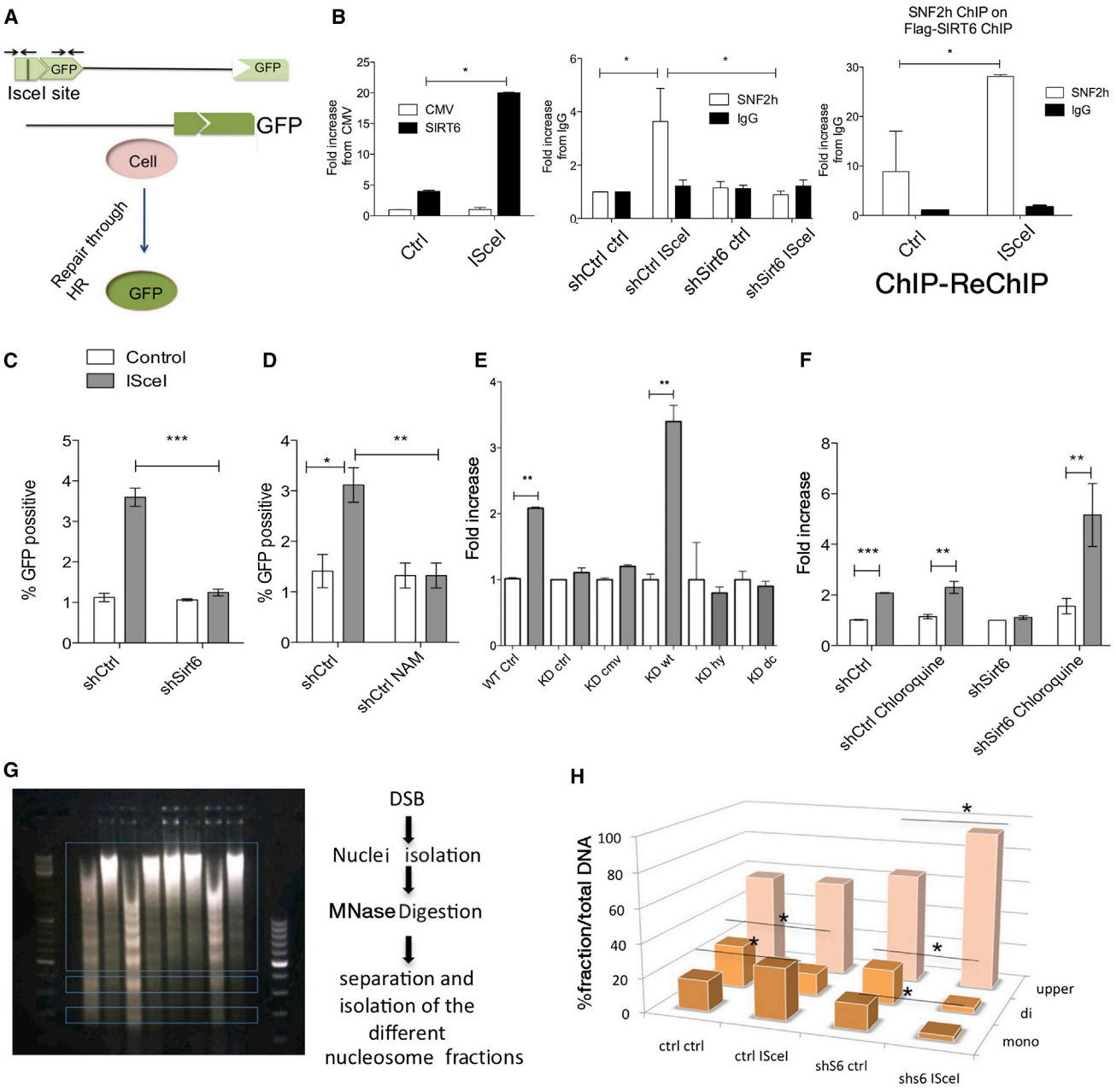

Figure 4. SIRT6 Modulates SNF2H-Dependent DSB Chromatin Opening and Repair

(A) Schematic representation of the DR-GFP/ISce-I system.

(B) Left panel: ChIP of cells transfected with Flag-cmv empty vector or Flag-S6 with or without I-SceI transfection. Middle panel: ChIP of SNF2H in shCtrl or shSIRT6 cells with or without Isce-I transfection. Right panel: sequential ChIP from Flag-SIRT6-eluted chromatin (ctrl or I-scel treated), where SNF2H or immunoglobulin G (IgG) was used for the second ChIP.

(C–F) HR efficiency measured by GFP-positive cells in shCtrl versus shSIRT6 (C); NAM-treated cells (10 mg/ml, 12 hr) (D); SIRT6-KD cells transfected with either WT-SIRT6, the catalytic mutant SIRT6-HY (catalytically inactive), or the C terminus-deleted (non-SNF2H interacting) SIRT6 fragments (E); and shCtrl and shSIRT6 cells pretreated for 2 hr with chloroquine (F).

(G) Chromatin accessibility at DNA breaks. Scheme of the experiment: DSBs were induced with the I-SceI endonuclease; nuclei were isolated and digested with MNase. Different nucleosomal fractions (mono, di, and upper) were separated on an agarose gel, and the abundance of the I-SceI site in the isolated DNA of each fraction was quantified using specific primers adjacent to the breaks.

(H) qPCR of the isolated DNA from the nucleosomes with primers adjacent to the damage site in shCtrl cells versus shSIRT6 cells. Data are represented as mean ± SEM. *$p < 0.05$, **$p < 0.01$, ***$p < 0.001$. See also Figure S4.

sites (Miller et al., 2010; Tjeertes et al., 2009; Yuan et al., 2009). Therefore, we tested whether SIRT6 functions as a H3K56 deacetylase at damage sites. ChIP with an anti-H3K56Ac antibody showed increased overall levels of H3K56 acetylation in shSIRT6 cells at damage sites (data not shown). Thus, we took advantage of our laser-induced DNA damage approach to determine whether SIRT6 was required to deacetylate H3K56 at break sites. We observed that H3K56Ac was clearly reduced in control cells within 7 min following laser-induced damage (Figure 5A), confirming previously published results (Miller et al., 2010; Tjeertes et al., 2009; Yuan et al., 2009). In contrast, such H3K56 deacetylation was barely observed in shSIRT6 cells (Figure 5A). To evaluate the impact of this modification on DSB repair, we transfected U2OS DR-GFP cells with a vector expressing a mutant form of histone H3 (H3K56Q) in which the K56 lysine residue was mutated to glutamine, an acetyl mimetic, and measured HR efficiency. Expression of the H3K56Q mutant impaired repair compared to WT H3K56-transfected cells (Figure 5B). These results suggest that SNF2H is unable to open chromatin when H3K56 cannot be deacetylated, highlighting a critical role for SIRT6 activity at damage sites, both as a recruiter of SNF2H and as a histone H3K56 deacetylase.

Lack of SIRT6 Impairs Downstream DDR Signaling

SIRT6 recruitment of SNF2H and H3K56 deacetylation appear to represent very early events in the DSB repair process. To evaluate downstream effects of SIRT6 deficiency, we analyzed recruitment of known DNA repair factors, taking advantage of a high-throughput microscope kinetic analysis of foci number (Figure S5). Recruitment kinetics were measured in shCtrl and shSIRT6 cells by immunostaining DNA repair signaling factors, including 53BP1, γH2AX, and RPA, at different time points after damage induction by IR. In U2OS shSIRT6 cells, formation of 53BP1 and γH2AX foci was impaired starting at 5 min, while a reduced number of RPA foci appeared at a later time point (30 min) (Figures 5C and 5D). In addition, we performed a comet assay in nonalkaline conditions (to measure double-strand break repair) and followed repair kinetics. In this assay, we observed a statistically significant increase in the tail length following damage in SIRT6-deficient cells at every time point we measured (Figure 5F), supporting our previous results demonstrating decreased DNA repair in shSIRT6 cells. Further, these results indicate that the reduced foci formation in these cells is not due to less damage, but rather reflects inefficient signaling at DSBs.

Using the laser-induced DNA damage assay, we showed that shSIRT6 cells exhibit a clear reduction in recruitment of replication protein A (RPA), 53BP1, and breast cancer 1 (BRCA1) to laser-induced breaks, consistent with the above results (Figures 6A–6D). The few positive cells denoted significantly less recruitment. As a control, no changes were seen for ATM phosphorylation at break sites (Figure 6A). Notably, shSNF2H cells showed a similar decrease in DDR factor recruitment, a phenotype that was not further reduced when both proteins were silenced (Figures 6A–6D). Overall, these results indicate that lack of SIRT6 profoundly impacts downstream recruitment of DNA repair factors, suggesting that both H3K56 deacetylation and SNF2H chromatin remodeling play critical roles in the DSB DNA repair pathway.

Lack of SIRT6 Increases DNA Damage In Vivo in a SNF2H-Dependent Manner

In order to test whether the effect of SIRT6 on DNA repair was physiologically relevant, we analyzed SNF2H and DNA damage responses in SIRT6-deficient mice. For this purpose, we isolated chromatin fractions from different tissues, including liver, heart, pancreas, and brain. Remarkably, we observed significantly decreased SNF2H chromatin localization in SIRT6-deficient brain and pancreas (Figures 6A and S7A), but not liver or heart (Figures S7B and S7C). Thus, SIRT6-dependent recruitment of SNF2H to chromatin appears to be tissue specific. To determine the importance of SIRT6 in DNA damage repair in vivo, we focused on the brain, where DNA damage may accumulate in postmitotic neurons. In addition, previous studies reported that brain-specific SIRT6 KO mice exhibit growth defects (Schwer et al., 2010), indicating that SIRT6 appears to play an important role in brain function. Notably, SIRT6-deficient brains (and pancreas) exhibited increased caspase-3 cleavage, p53 phosphorylation, PARP cleavage, ATM phosphorylation, and, consistently, increased H3K56Ac levels (Figures 7A, 7B, and S7A–S7C). We then generated primary brain cultures from WT and SIRT6 KO mice and measured the presence of RPA and 53BP1 foci following irradiation. Primary brain cultures from SIRT6 KO mice had reduced 53BP1 and RPA foci at 30 min (Figures 7C–7E), similar to the effect observed in shSIRT6 U2OS cells (Figures 5C, 5D, 6B, and 6C). In summary, these results indicate that SIRT6-deficient animals experience increased DNA damage in the brain, a phenotype strongly correlated with defective H3K56 deacetylation and recruitment of SNF2H to chromatin.

DISCUSSION

SIRT6 is a chromatin-bound enzyme that was first described as a suppressor of genomic instability by regulating base excision DNA repair (BER) (Mostoslavsky et al., 2006). Recent studies have demonstrated that SIRT6 is involved in DNA double-strand break resection through deacetylation of C-terminal-binding protein (CtBP)-interacting protein (CtIP) (Kaidi et al., 2010), increase in repair capacity under oxidative stress through PARP1 (Mao et al., 2011), and stabilization of DNA-PK at damage sites (McCord et al., 2009). Here, we demonstrate that SIRT6 is one of the most rapidly recruited factors to DNA damage sites. Such fast recruitment may allow SIRT6 to coordinate proper DNA repair through a complex and step-wise response (see model in Figure 7F). Our results extend previously proposed roles for SIRT6 in DDR and reveal that SIRT6 plays a critical role in regulating chromatin accessibility as a very early event during the DNA damage response. This activity involves direct recruitment of the ATP-dependent chromatin remodeler SNF2H to DNA break sites and in parallel rapid histone deacetylation at histone H3K56 to allow recruitment of downstream DNA repair factors. Our results represent a unique example of a sirtuin deacetylase functioning as a specific scaffold for recruiting a chromatin remodeler to DNA damage sites to open chromatin and repair DNA breaks in a coordinated manner.

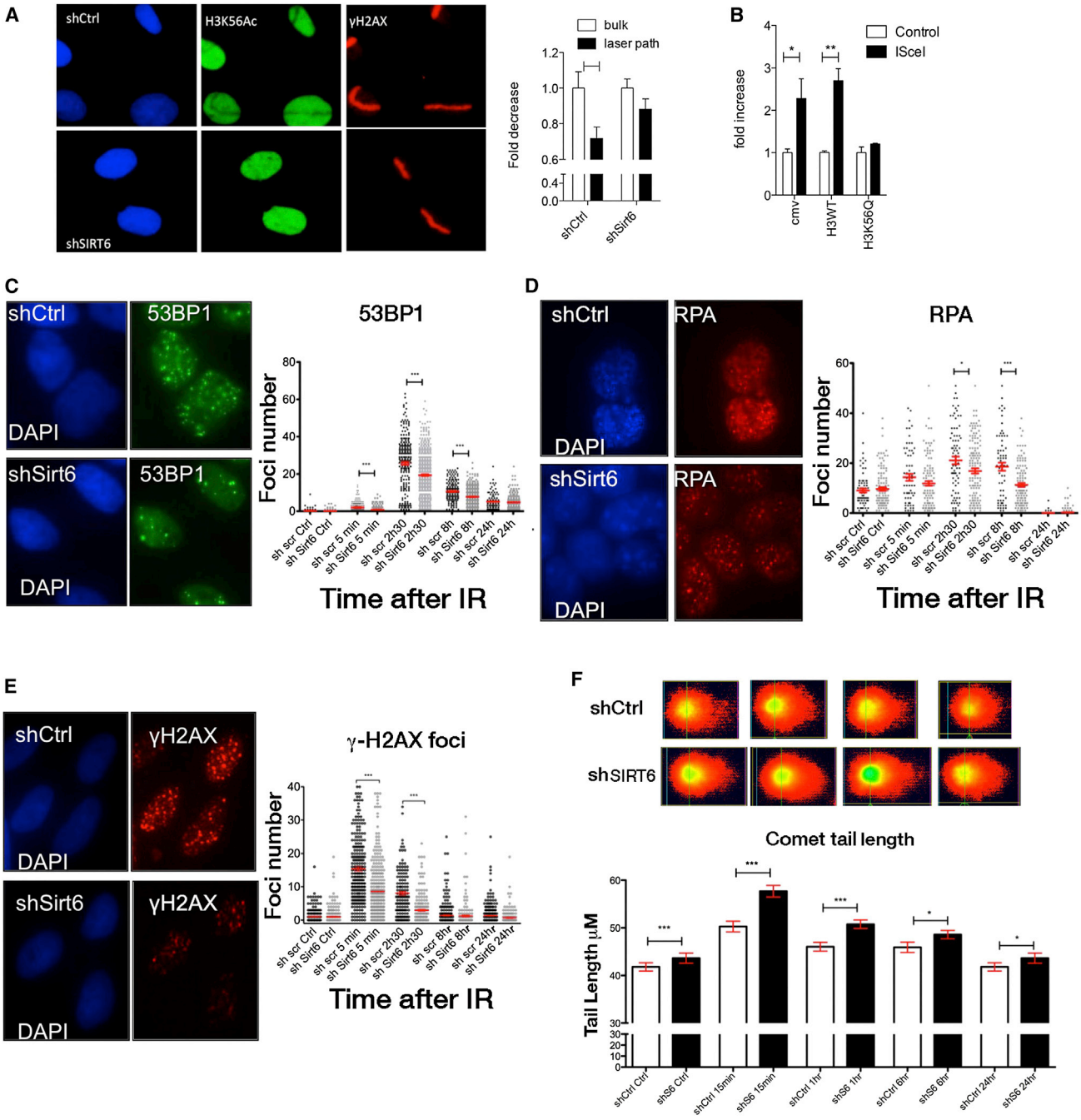

Figure 5. SIRT6 Modulates H3K56 Deacetylation and Recruitment of Repair Factors at DSBs

(A) Immunofluorescence showing H3K56Ac at damage sites after laser-induced damage in shCtrl and shSIRT6 U2OS cells. H3K56Ac levels were measured at and beside damage sites. Data are represented as mean ± SEM.

(B) Quantification of GFP-positive U2OS-DR-GFP cells transfected with H3-WT or H3K56Q mutant.

(C–E) High-throughput analysis of foci number showing 53BP1 (C), RPA (D), and γH2AX (E) foci number per cell at different time points after IR in shCtrl versus shSIRT6 U2OS cells.

(F) Comet tail length for shCtrl and shSIRT6 is quantified at the indicated time points. Representative pictures are shown (15 min time point). Data are represented as mean ± SEM. P values are abbreviated as in Figure 4. See also Figure S5.

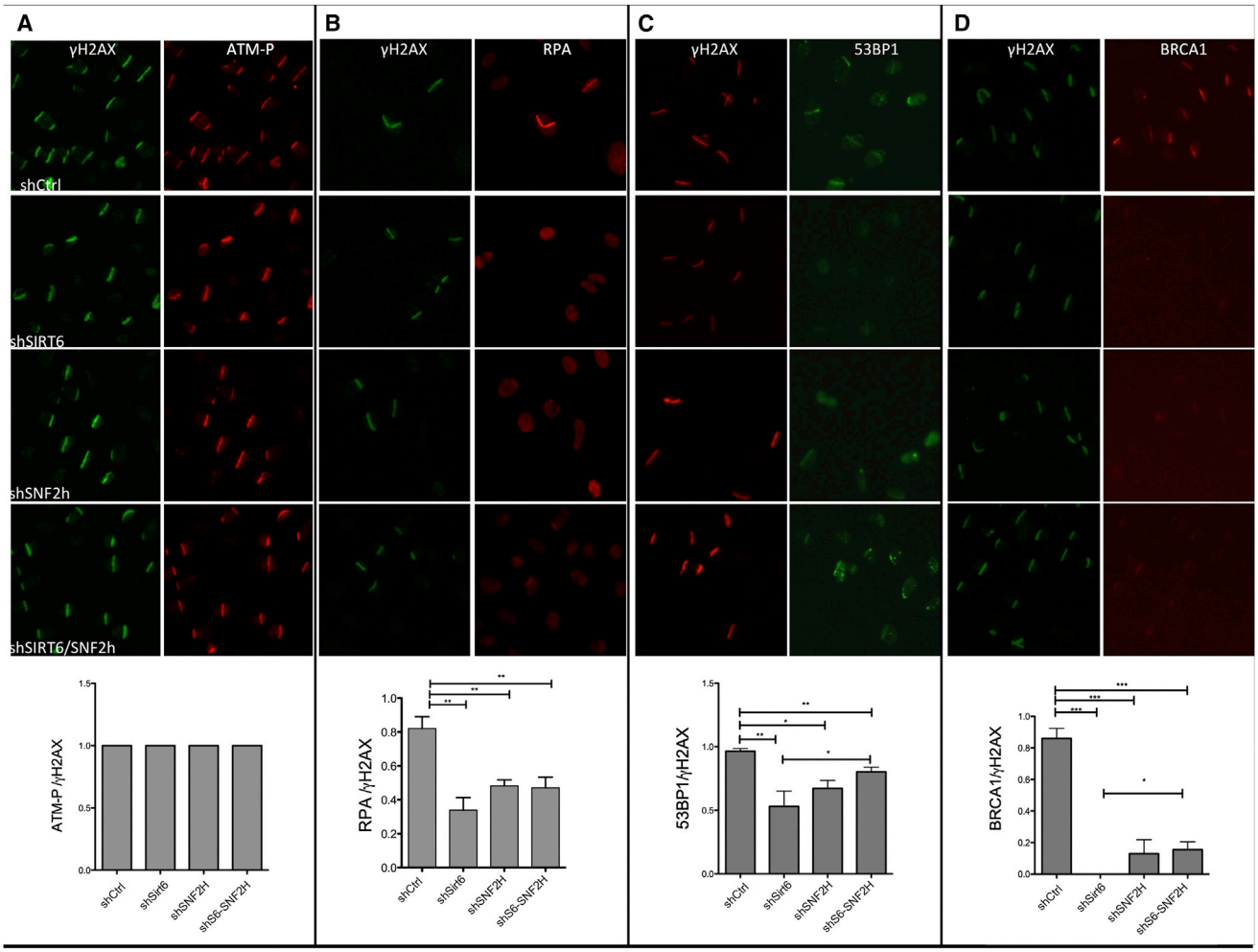

Figure 6. Decreased Recruitment of Repair Factors to Laser-Induced Breaks in the Absence of SIRT6

(A–D) Following laser-induced damage, recruitment of ATM-P (A), RPA (B), 53BP1 (C), and BRCA1 (D) was quantified in the indicated genotypes. Data are represented as mean ± SEM. See also Figure S6.

SIRT6 and SNF2H Are Recruited Early to DNA Damage Sites to Modulate Chromatin Accessibility

Our results show that the interaction between SNF2H and SIRT6 is important to bind SNF2H to chromatin, even at basal levels (Figure 2A). It has been previously proposed that SNF2H probes the chromatin through continuous sampling until it recognizes an anchoring signal, which in turn increases SNF2H binding affinity (Erdel and Rippe, 2011). We believe that SIRT6 is one of those signals, as it increases SNF2H binding to nucleosomes (Figure 1H), and this chromatin-bound complex might have additional functions beyond DNA repair. However, the interaction of both proteins, and thus the abundance of this complex, is clearly increased upon DNA damage. Our results indicate that SNF2H and SIRT6 work in an epistatic manner to prevent genomic instability (Figures 2F, 2G, and 6A–6D). Remarkably, recruitment of SIRT6 appears extremely early (~5 s with an ~30 s plateau), positioning SIRT6 as one of the earliest factors to accumulate at DNA damage sites, followed by SNF2H, which is only recruited to DSBs in the presence of SIRT6 (Figures 3A–3E and 4B). Our experiments in living cells demonstrate that SIRT6 and SNF2H are both recruited very early, whereas SIRT6 appears to modulate the second, more stable phase of SNF2H binding specifically at DSBs. Early, transient binding of SNF2H occurs independently of SIRT6 and may represent SNF2H recruitment to other types of DNA lesions.

SIRT6 Activity Is Required for Proper DNA Repair

Although SIRT6 activity is not required to bring SNF2H to chromatin (Figure 2C), or to control SNF2H remodeling activity in vitro, both SIRT6 deacetylase activity and recruitment of SNF2H were required for efficient DNA repair (Figures 4D and 4E). The role of H3K56 acetylation in DNA damage has been controversial, with some studies reporting hypoacetylation of H3K56 at breaks sites (Miller et al., 2010; Tjeertes et al., 2009), whereas others showed hyperacetylation following DNA damage (Das et al., 2009). In addition, both class I histone

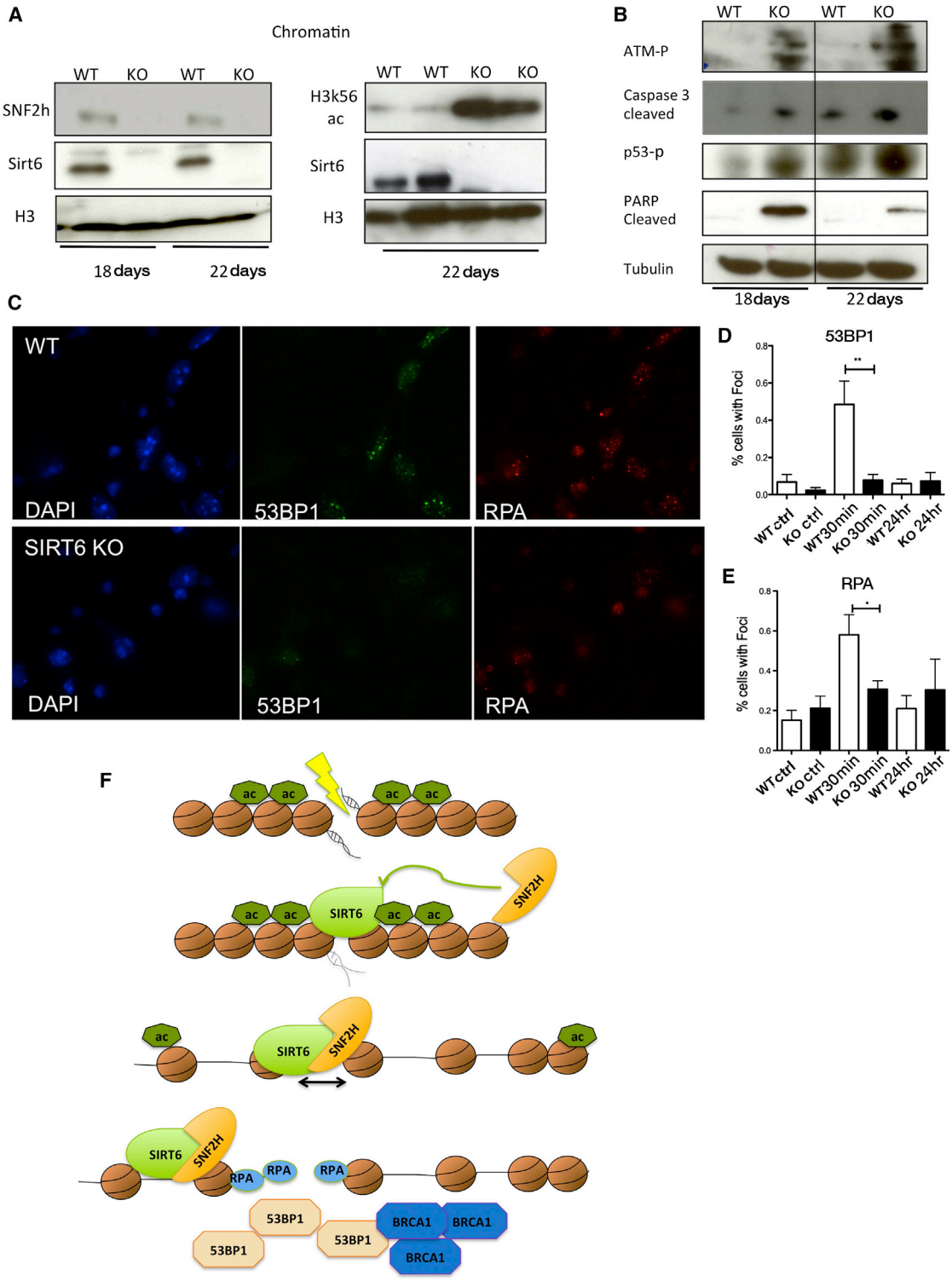

Figure 7. SIRT6 Modulates SNF2H Recruitment and DNA Repair In Vivo

(A and B) Chromatin fractions or whole-cell extracts from brains of 18- or 22-day-old mice from WT or SIRT6 KO animals with the noted antibodies.

(C) Primary brain cells cultured for 14 days before damage and collected at different time points (30 min after IR is shown) for RPA and 53BP1.

(D and E) Quantification of 53BP1 (D) and RPA (E) foci.

(F) Proposed model: SIRT6 is mobilized to the damage sites very early, recruiting SNF2H and deacetylating H3K56, allowing opening of chromatin and recruitment of downstream repair factors such as 53BP1, RPA, and BRCA1. Data are represented as mean ± SEM. *$p < 0.05$, **$p < 0.001$. See also Figure S7.

deacetylases (HDACs) and sirtuins are capable of deacetylating H3K56 (Michishita et al., 2009; Miller et al., 2010; Yang et al., 2009). Our results indicate that SIRT6 is critical for proper deacetylation of H3K56 at damage sites in our experimental conditions (Figure 5A). Some of the discrepancies may be due to the timescale of the measurement, type of DNA damage, and specific cells tested. In our system, we observed clear hypoacetylation at early time points (~7 min) but detected bulk H3K56 hyperacetylation at very late time points (6–8 hr, data not shown), a potential late remodeling required for proper refolding of chromatin following repair, as seen in yeast (Chen et al., 2008). Notably, several HDACs have been shown to play roles in DNA repair. Indeed, we observed increased H3K56Ac following trichostatin A (TSA) treatment. However, this increase did not influence recruitment of SNF2H to chromatin (data not shown). These results indicate that SNF2H recruitment specifically depends on SIRT6 and is not regulated by other HDACs or the H3K56Ac modification per se. Furthermore, the fact that we observe a clear repair defect in the absence of SIRT6 strongly suggests nonoverlapping or redundant functions with other HDACs.

SIRT6 Affects Downstream DDR Signaling

Our results show that lack of SIRT6 influences recruitment of downstream repair factors such as 53BP1, γH2AX, RPA, and BRCA1. In our shCtrl and shSIRT6 cells, this was independent of the cell cycle stage, in agreement with previous findings by Kaidi et al. (2010). Taken together, our results indicate that chromatin remodeling and early histone modifications have a profound impact on recruitment of downstream effectors. Previous work has shown that lack of 53BP1 increases end resection and RPA foci (Bunting et al., 2010). Therefore, one may hypothesize that decreased 53BP1 foci in SIRT6-deficient cells should increase RPA foci. However, given the previously published effect of SIRT6 on CtIP (Kaidi et al., 2010), it is likely that end resection is inhibited in the absence of SIRT6; thus, both RPA and 53BP1 cannot be recruited. Consistently, cells deficient in the remodelers INO80 and SMARCAD1 exhibited defective DNA end resection and a concomitant lack of both RPA and 53BP1 foci (Costelloe et al., 2012).

Previous studies have shown that SNF2H recruitment occurs downstream of histone H2B K120 ubiquitylation (H2B K120Ub) by RNF20 (Nakamura et al., 2011). Interestingly, in SIRT6 KO cells and tissues, RNF20 recruitment to chromatin was clearly impaired. Further, H2B K120Ub was severely diminished in SIRT6-deficient cells (Figures S6A and S6B), suggesting that these events occur downstream of SIRT6. Notably, Smeenk et al. (2013) showed that SNF2H spreading on chromatin was dependent on PARP1 activity, and SIRT6 was recently shown to activate PARP1 under oxidative damage conditions (Mao et al., 2011). These results suggest that SNF2H spreading could also be affected by lack of SIRT6 through a PARP1-dependent mechanism. However, in our system, we did not observe defects in SNF2H spreading (Figure S4F) or on PAR levels at DNA damage sites (Figures S6D and S6E) in the absence of SIRT6, indicating that the previously published role for SIRT6 in modulating PARP1 activity might be specific for oxidative DNA damage.

Lack of SIRT6 Increases Vulnerability to DNA Damage in a Tissue-Specific Manner

The roles of SIRT6 in DNA damage repair are physiologically relevant, since SIRT6-deficient brains exhibited a clear decrease in chromatin-localized SNF2H and increased DNA damage (Figures 7A–7E), a phenotype also observed in other tissues such as pancreas (Figure S7A). Proper DNA repair is critical to prevent neurodegeneration, cancer, and premature aging. Indeed, recent studies have shown that SIRT6 overexpression extends lifespan (Kanfi et al., 2012), and deleting SIRT6 specifically in the brain causes metabolic abnormalities (Schwer et al., 2010). Further, recent studies indicate that SIRT6 can function as a tumor suppressor, at least in part through modulation of metabolism (Sebastián et al., 2012). Intriguingly, SIRT6 protein levels in these different tissues do not correlate with the DNA damage phenotype (Liszt et al., 2005; Mostoslavsky et al., 2006), suggesting that tissue specificity is not based on SIRT6 levels, but rather on either as-of-yet unknown cofactors or redundancy with other proteins able to recruit SNF2H. Based on the results presented here, we conclude that the SIRT6 chromatin scaffolding function is essential for preventing genomic instability and may explain several of the phenotypes previously associated to SIRT6.

EXPERIMENTAL PROCEDURES

Immunoprecipitation

Cells were lysed and sonicated for 15 min (with intervals of 1 s on, 3 s off) in lysis buffer (10 mM Tris [pH 7.9], 150 mM KCL, and protease, deacetylase, and phosphatase inhibitors). Protein was precleared for 2 hr with beads at 4°C and left overnight with blocked beads (5% BSA) and the desired antibody. Beads were washed 2 times with 150 mM KCL, 2 times with 300 mM KCL, and 1 time with 150 mM KCL, and proteins were eluted either by flag peptide/or boiling.

MNase Assay qPCR

shControl or shSIRT6 U2OS cells (2×10^6) were transfected with a plasmid carrying the I-SceI site (I-SceI-pBSK, a kind gift from F. Alt) (Wang et al., 2009). After 48 hr, cells with or without the I-SceI enzyme were homogenized with a Dounce homogenizer in reticulocyte standard buffer (RSB) (10 mM Tris-HCl [pH 7.4], 10 mM NaCl, 3 mM $MgCl_2$, 0.5% NP-40, 1 mM phenylmethylsulfonyl fluoride (PMSF), 1 mM dithiothreitol (DTT), and protease inhibitors). Cells were incubated on ice for 15 min, and nuclei were collected by centrifugation at 1,000 × *g*) for 10 min at 4°C, washed twice with RSB, and digested with MNase in digestion buffer at room temperature (RT) (140 units, time course from 5–20 min). Reaction was stopped by adding 1 volume of Stop Solution (50 mM Tris-HCl [pH 7.5],150 mM NaCl, 50 mM EDTA, 0.3% SDS). Samples were centrifuged at 10,000 × *g* for 10 min at 4°C. DNA was purified by phenol-chloroform extraction and resolved in a 2% agarose gel. Bands were isolated and purified using a Gel Extraction Kit (QIAGEN). Extracted DNA was used in qPCR reactions as indicated.

Nuclear IP

Nuclei were isolated from cells and treated with 2 units of MNase for 1 hr at room temperature. The MNase reaction was stopped, and protein was measured with Bradford to proceed with the IP as described before.

Primary Cortical Cell Culture

Cortex and hippocampus were separated from 18-day-old SIRT6 WT and KO embryos and minced, and cells were plated on poly-L-ornithine-coated coverslips in Neurobasal medium, B27 supplement, GlutaMAX, and penicillin/streptomycin (Invitrogen). Tail DNA was used to genotype the embryos. All mouse experiments were performed under an IACUC-approved protocol.

SUPPLEMENTAL INFORMATION

Supplemental Information includes Supplemental Experimental Procedures and seven figures and can be found with this article online at http://dx.doi.org/10.1016/j.molcel.2013.06.018.

ACKNOWLEDGMENTS

This work was supported in part by NIH grant GM093072-01 (R.M.). R.M is a Howard Goodman Scholar Awardee and an MGH Research Scholar. D.T. is the recipient of the Brain Power for Israel Foundation grant and the Ellison Medical Foundation/AFAR Postdoctoral Fellowship. C.C. is supported by a Fellowship from the Fondazione Umberto Veronesi. C.S. is the recipient of a CDMRP/DoD Cancer Research Program Postdoctoral Fellowship. B.M.-P is the recipient of a postdoctoral fellowship from the Spanish Ministry of Education. We would like to thank Steve Jackson for the SIRT6-GFP and SIRT6-RFP plasmids and Laura Prickett-Rice and Kate Folz-Donahue for technical assistance with the FACS analysis.

Received: January 29, 2013
Revised: May 16, 2013
Accepted: June 24, 2013
Published: August 1, 2013

REFERENCES

Bunting, S.F., Callén, E., Wong, N., Chen, H.T., Polato, F., Gunn, A., Bothmer, A., Feldhahn, N., Fernandez-Capetillo, O., Cao, L., et al. (2010). 53BP1 inhibits homologous recombination in Brca1-deficient cells by blocking resection of DNA breaks. Cell *141*, 243–254.

Chapman, J.R., Taylor, M.R., and Boulton, S.J. (2012). Playing the end game: DNA double-strand break repair pathway choice. Mol. Cell *47*, 497–510.

Chen, C.C., Carson, J.J., Feser, J., Tamburini, B., Zabaronick, S., Linger, J., and Tyler, J.K. (2008). Acetylated lysine 56 on histone H3 drives chromatin assembly after repair and signals for the completion of repair. Cell *134*, 231–243.

Chen, X., Cui, D., Papusha, A., Zhang, X., Chu, C.D., Tang, J., Chen, K., Pan, X., and Ira, G. (2012). The Fun30 nucleosome remodeller promotes resection of DNA double-strand break ends. Nature *489*, 576–580.

Ciccia, A., and Elledge, S.J. (2010). The DNA damage response: making it safe to play with knives. Mol. Cell *40*, 179–204.

Costelloe, T., Louge, R., Tomimatsu, N., Mukherjee, B., Martini, E., Khadaroo, B., Dubois, K., Wiegant, W.W., Thierry, A., Burma, S., et al. (2012). The yeast Fun30 and human SMARCAD1 chromatin remodellers promote DNA end resection. Nature *489*, 581–584.

Das, C., Lucia, M.S., Hansen, K.C., and Tyler, J.K. (2009). CBP/p300-mediated acetylation of histone H3 on lysine 56. Nature *459*, 113–117.

Erdel, F., and Rippe, K. (2011). Chromatin remodelling in mammalian cells by ISWI-type complexes—where, when and why? FEBS J. *278*, 3608–3618.

Erdel, F., Schubert, T., Marth, C., Längst, G., and Rippe, K. (2010). Human ISWI chromatin-remodeling complexes sample nucleosomes via transient binding reactions and become immobilized at active sites. Proc. Natl. Acad. Sci. USA *107*, 19873–19878.

Finkel, T., Deng, C.X., and Mostoslavsky, R. (2009). Recent progress in the biology and physiology of sirtuins. Nature *460*, 587–591.

Gospodinov, A., Vaissiere, T., Krastev, D.B., Legube, G., Anachkova, B., and Herceg, Z. (2011). Mammalian Ino80 mediates double-strand break repair through its role in DNA end strand resection. Mol. Cell. Biol. *31*, 4735–4745.

Kaidi, A., Weinert, B.T., Choudhary, C., and Jackson, S.P. (2010). Human SIRT6 promotes DNA end resection through CtIP deacetylation. Science *329*, 1348–1353.

Kanfi, Y., Naiman, S., Amir, G., Peshti, V., Zinman, G., Nahum, L., Bar-Joseph, Z., and Cohen, H.Y. (2012). The sirtuin SIRT6 regulates lifespan in male mice. Nature *483*, 218–221.

Kashiwaba, S., Kitahashi, K., Watanabe, T., Onoda, F., Ohtsu, M., and Murakami, Y. (2010). The mammalian INO80 complex is recruited to DNA damage sites in an ARP8 dependent manner. Biochem. Biophys. Res. Commun. *402*, 619–625.

Kielbassa, C., Roza, L., and Epe, B. (1997). Wavelength dependence of oxidative DNA damage induced by UV and visible light. Carcinogenesis *18*, 811–816.

Lan, L., Ui, A., Nakajima, S., Hatakeyama, K., Hoshi, M., Watanabe, R., Janicki, S.M., Ogiwara, H., Kohno, T., Kanno, S., and Yasui, A. (2010). The ACF1 complex is required for DNA double-strand break repair in human cells. Mol. Cell *40*, 976–987.

Larsen, D.H., Poinsignon, C., Gudjonsson, T., Dinant, C., Payne, M.R., Hari, F.J., Rendtlew Danielsen, J.M., Menard, P., Sand, J.C., Stucki, M., et al. (2010). The chromatin-remodeling factor CHD4 coordinates signaling and repair after DNA damage. J. Cell Biol. *190*, 731–740.

Lee, H.S., Park, J.H., Kim, S.J., Kwon, S.J., and Kwon, J. (2010). A cooperative activation loop among SWI/SNF, gamma-H2AX and H3 acetylation for DNA double-strand break repair. EMBO J. *29*, 1434–1445.

Liszt, G., Ford, E., Kurtev, M., and Guarente, L. (2005). Mouse Sir2 homolog SIRT6 is a nuclear ADP-ribosyltransferase. J. Biol. Chem. *280*, 21313–21320.

Lukas, J., Lukas, C., and Bartek, J. (2011). More than just a focus: The chromatin response to DNA damage and its role in genome integrity maintenance. Nat. Cell Biol. *13*, 1161–1169.

Mao, Z., Hine, C., Tian, X., Van Meter, M., Au, M., Vaidya, A., Seluanov, A., and Gorbunova, V. (2011). SIRT6 promotes DNA repair under stress by activating PARP1. Science *332*, 1443–1446.

McCord, R.A., Michishita, E., Hong, T., Berber, E., Boxer, L.D., Kusumoto, R., Guan, S., Shi, X., Gozani, O., Burlingame, A.L., et al. (2009). SIRT6 stabilizes DNA-dependent protein kinase at chromatin for DNA double-strand break repair. Aging (Albany NY) *1*, 109–121.

Michishita, E., McCord, R.A., Boxer, L.D., Barber, M.F., Hong, T., Gozani, O., and Chua, K.F. (2009). Cell cycle-dependent deacetylation of telomeric histone H3 lysine K56 by human SIRT6. Cell Cycle *8*, 2664–2666.

Miller, K.M., Tjeertes, J.V., Coates, J., Legube, G., Polo, S.E., Britton, S., and Jackson, S.P. (2010). Human HDAC1 and HDAC2 function in the DNA-damage response to promote DNA nonhomologous end-joining. Nat. Struct. Mol. Biol. *17*, 1144–1151.

Mostoslavsky, R., Chua, K.F., Lombard, D.B., Pang, W.W., Fischer, M.R., Gellon, L., Liu, P., Mostoslavsky, G., Franco, S., Murphy, M.M., et al. (2006). Genomic instability and aging-like phenotype in the absence of mammalian SIRT6. Cell *124*, 315–329.

Murr, R., Loizou, J.I., Yang, Y.G., Cuenin, C., Li, H., Wang, Z.Q., and Herceg, Z. (2006). Histone acetylation by Trrap-Tip60 modulates loading of repair proteins and repair of DNA double-strand breaks. Nat. Cell Biol. *8*, 91–99.

Nakamura, K., Kato, A., Kobayashi, J., Yanagihara, H., Sakamoto, S., Oliveira, D.V., Shimada, M., Tauchi, H., Suzuki, H., Tashiro, S., et al. (2011). Regulation of homologous recombination by RNF20-dependent H2B ubiquitination. Mol. Cell *41*, 515–528.

Neumann, F.R., Dion, V., Gehlen, L.R., Tsai-Pflugfelder, M., Schmid, R., Taddei, A., and Gasser, S.M. (2012). Targeted INO80 enhances subnuclear chromatin movement and ectopic homologous recombination. Genes Dev. *26*, 369–383.

Papamichos-Chronakis, M., and Peterson, C.L. (2013). Chromatin and the genome integrity network. Nat. Rev. Genet. *14*, 62–75.

Papamichos-Chronakis, M., Watanabe, S., Rando, O.J., and Peterson, C.L. (2011). Global regulation of H2A.Z localization by the INO80 chromatin-remodeling enzyme is essential for genome integrity. Cell *144*, 200–213.

Pierce, A.J., Hu, P., Han, M., Ellis, N., and Jasin, M. (2001). Ku DNA end-binding protein modulates homologous repair of double-strand breaks in mammalian cells. Genes Dev. *15*, 3237–3242.

Polo, S.E., Kaidi, A., Baskcomb, L., Galanty, Y., and Jackson, S.P. (2010). Regulation of DNA-damage responses and cell-cycle progression by the chromatin remodelling factor CHD4. EMBO J. *29*, 3130–3139.

Schwer, B., Schumacher, B., Lombard, D.B., Xiao, C., Kurtev, M.V., Gao, J., Schneider, J.I., Chai, H., Bronson, R.T., Tsai, L.H., et al. (2010). Neural sirtuin 6 (Sirt6) ablation attenuates somatic growth and causes obesity. Proc. Natl. Acad. Sci. USA *107*, 21790–21794.

Sebastián, C., Zwaans, B.M., Silberman, D.M., Gymrek, M., Goren, A., Zhong, L., Ram, O., Truelove, J., Guimaraes, A.R., Toiber, D., et al. (2012). The histone deacetylase SIRT6 is a tumor suppressor that controls cancer metabolism. Cell *151*, 1185–1199.

Smeenk, G., Wiegant, W.W., Vrolijk, H., Solari, A.P., Pastink, A., and van Attikum, H. (2010). The NuRD chromatin-remodeling complex regulates signaling and repair of DNA damage. J. Cell Biol. *190*, 741–749.

Smeenk, G., Wiegant, W.W., Marteijn, J.A., Luijsterburg, M.S., Sroczynski, N., Costelloe, T., Romeijn, R.J., Pastink, A., Mailand, N., Vermeulen, W., et al. (2013). Poly(ADP-ribosyl)ation links the chromatin remodeler SMARCA5/SNF2H to RNF168-dependent DNA damage signaling. J. Cell Sci. *126*, 889–903. Published online December 21, 2012. http://dx.doi.org/10.1242/jcs.109413.

Tennen, R.I., Berber, E., and Chua, K.F. (2010). Functional dissection of SIRT6: identification of domains that regulate histone deacetylase activity and chromatin localization. Mech. Ageing Dev. *131*, 185–192.

Tjeertes, J.V., Miller, K.M., and Jackson, S.P. (2009). Screen for DNA-damage-responsive histone modifications identifies H3K9Ac and H3K56Ac in human cells. EMBO J. *28*, 1878–1889.

Toiber, D., Sebastian, C., and Mostoslavsky, R. (2011). Characterization of nuclear sirtuins: molecular mechanisms and physiological relevance. Handb Exp Pharmacol *206*, 189–224.

Wang, J.H., Gostissa, M., Yan, C.T., Goff, P., Hickernell, T., Hansen, E., Difilippantonio, S., Wesemann, D.R., Zarrin, A.A., Rajewsky, K., et al. (2009). Mechanisms promoting translocations in editing and switching peripheral B cells. Nature *460*, 231–236.

Xu, Y., Sun, Y., Jiang, X., Ayrapetov, M.K., Moskwa, P., Yang, S., Weinstock, D.M., and Price, B.D. (2010). The p400 ATPase regulates nucleosome stability and chromatin ubiquitination during DNA repair. J. Cell Biol. *191*, 31–43.

Xu, Y., Ayrapetov, M.K., Xu, C., Gursoy-Yuzugullu, O., Hu, Y., and Price, B.D. (2012). Histone H2A.Z controls a critical chromatin remodeling step required for DNA double-strand break repair. Mol. Cell *48*, 723–733.

Yang, B., Zwaans, B.M., Eckersdorff, M., and Lombard, D.B. (2009). The sirtuin SIRT6 deacetylates H3 K56Ac in vivo to promote genomic stability. Cell Cycle *8*, 2662–2663.

Yuan, J., Pu, M., Zhang, Z., and Lou, Z. (2009). Histone H3-K56 acetylation is important for genomic stability in mammals. Cell Cycle *8*, 1747–1753.

Zhong, L., D'Urso, A., Toiber, D., Sebastian, C., Henry, R.E., Vadysirisack, D.D., Guimaraes, A., Marinelli, B., Wikstrom, J.D., Nir, T., et al. (2010). The histone deacetylase Sirt6 regulates glucose homeostasis via Hif1alpha. Cell *140*, 280–293.

Molecular Cell, Volume *51*

Supplemental Information

SIRT6 Recruits SNF2H to DNA Break Sites, Preventing Genomic Instability through Chromatin Remodeling

Debra Toiber, Fabian Erdel, Karim Bouazoune, Dafne M. Silberman, Lei Zhong, Peter Mulligan, Carlos Sebastian, Claudia Cosentino, Barbara Martinez-Pastor, Sofia Giacosa, Agustina D'Urso, Anders M. Näär, Robert Kingston, Karsten Rippe, and Raul Mostoslavsky

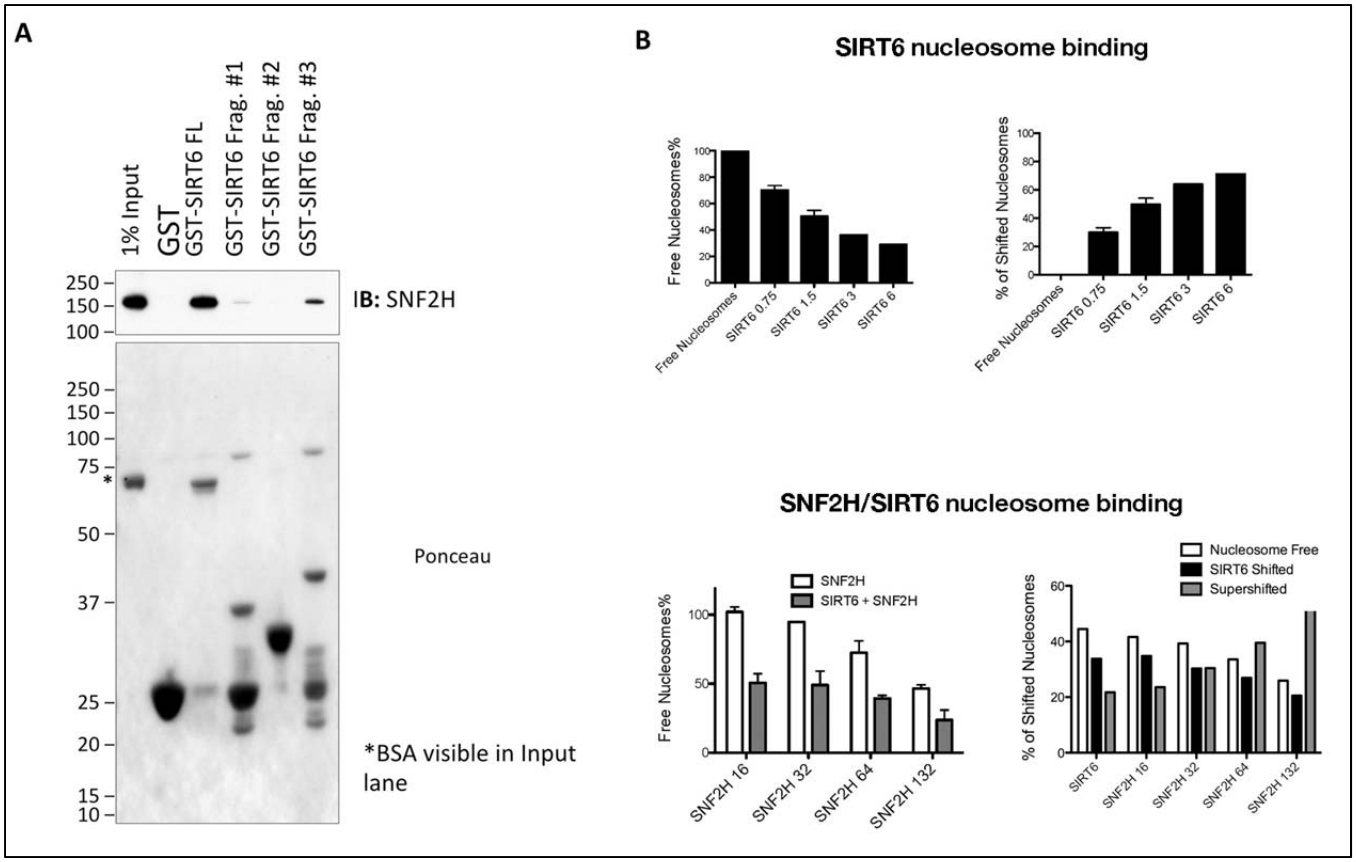

Figure S1. Related to Figure 1

A. GST-Purified SIRT6 proteins fragments showing interaction between SNF2H and the full length SIRT6 protein, a weak interaction with the N-terminus (#1), no interaction with the core (#2) and clear interaction with the C terminus (#3). **B.** Upper graphs: quantification of nucleosome binding by purified SIRT6 at the concentrations indicated (μM), as shown in Figure 1H. Left panel: free nucleosomes quantification when adding recombinant SNF2H (at indicated nM concentration) in the absence (white bars) or presence (gray bars) of SIRT6. Right panel: % of the indicated fractions/total DNA per lane, data is represented as mean +/- SEM.

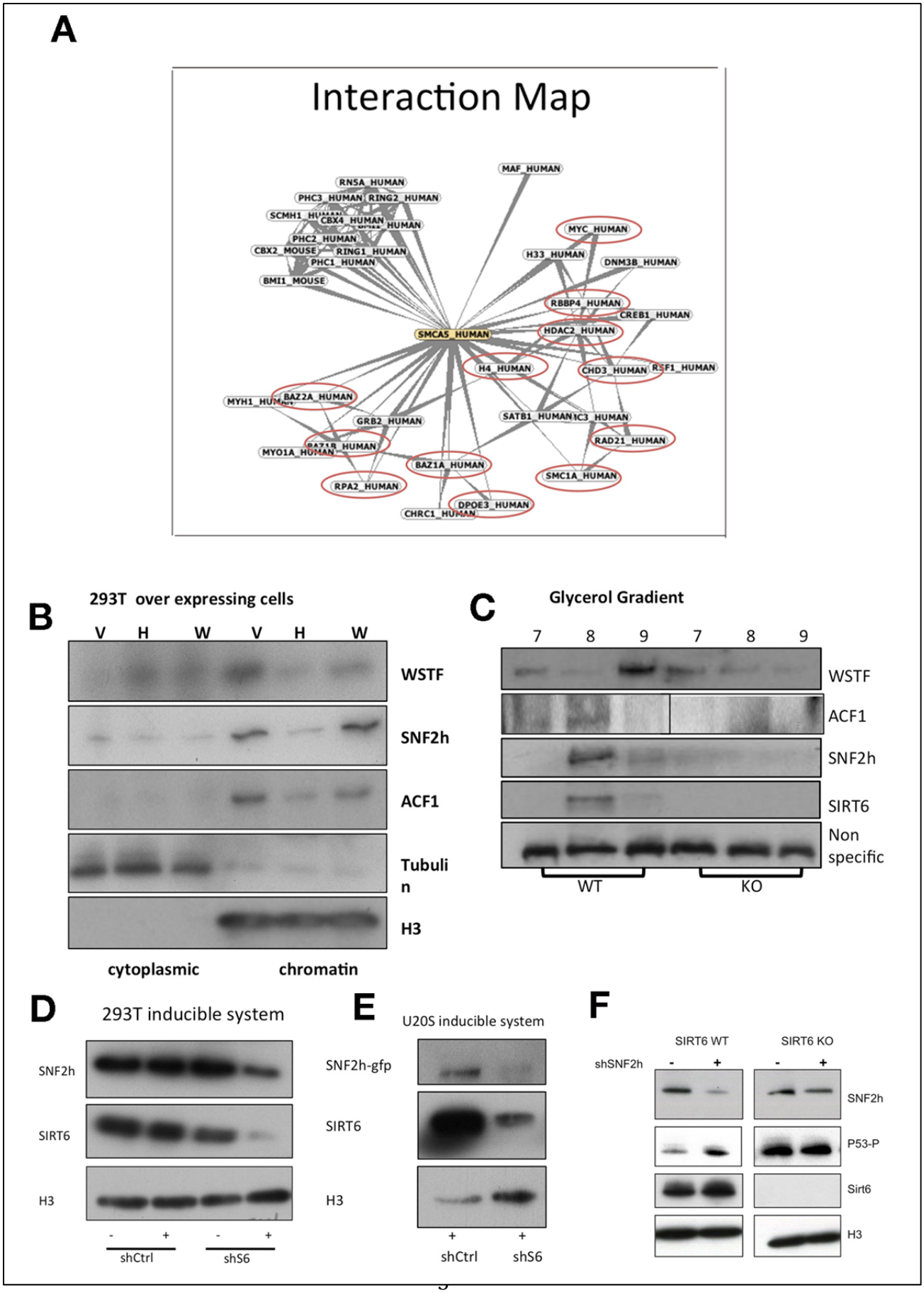
A
Interaction Map
MAF_HUMAN
RN5A_HUMAN
PHC3_HUMAN
RING2_HUMAN
SCMH1_HUMAN
CBX4_HUMAN
PHC2_HUMAN
CBX2_MOUSE
RING1_HUMAN
PHC1_HUMAN
BMI1_MOUSE
MYC_HUMAN
H33_HUMAN
DNM3B_HUMAN
RBBP4_HUMAN
CREB1_HUMAN
SMCA5_HUMAN
HDAC2_HUMAN
H4_HUMAN
CHD3_HUMAN
RSF1_HUMAN
MYH1_HUMAN
BAZ2A_HUMAN
GRB2_HUMAN
SATB1_HUMAN
RAD21_HUMAN
MYO1A_HUMAN
BAZ1A_HUMAN
SMC1A_HUMAN
RPA2_HUMAN
DPOE3_HUMAN
CHRC1_HUMAN
B
293T over expressing cells
V H W V H W
WSTF
SNF2h
ACF1
Tubulin
H3
cytoplasmic
chromatin
C
Glycerol Gradient
7 8 9 7 8 9
WSTF
ACF1
SNF2h
SIRT6
Non specific
WT
KO
D
293T inducible system
SNF2h
SIRT6
H3
- + - +
shCtrl
shS6
E
U20S inducible system
SNF2h-gfp
SIRT6
H3
+ +
shCtrl
shS6
F
SIRT6 WT
SIRT6 KO
shSNF2h
- + - +
SNF2h
P53-P
Sirt6
H3

Figure S2. Related to Figure 2

A) Depicted is the Agile Protein Interaction DataAnalyzer (APID), http://bioinfow.dep.usal.es/apid/ for SNF2H interactors map, red circles are marked proteins which were identified in the SIRT6 mass spec analysis. Note that it appears that only a subset of SNF2H interactors are also part of SIRT6 complexes. B) WSTF and ACF1 are buffered out from chromatin in the presence of SIRT6-HY, indicating that SIRT6, likely through SNF2H, modifies their localization. V: vector-transfected. H: SIRT6-HY transfected. W: SIRT6-WT transfected C) Glycerol gradient shows a similar pattern for ACF1 in the SIRT6 WT cells (fractions 7-9), and absence in the SIRT6 KO cells. While WSTF exhibits co-localization in some of the fractions, it remains in those fractions in the absence of SIRT6. D-E) Doxycycline inducible silencing of SIRT6 in 293T (D) and U2OS (E) cells after 72hrs of treatment. Western blots on chromatin fractions were performed with indicated antibodies. Note the clear decrease in SNF2H in chromatin following acute inhibition of SIRT6 expression. F) Western blot showing p53 phosphorylation in cells defective for SIRT6, SNF2H or both.

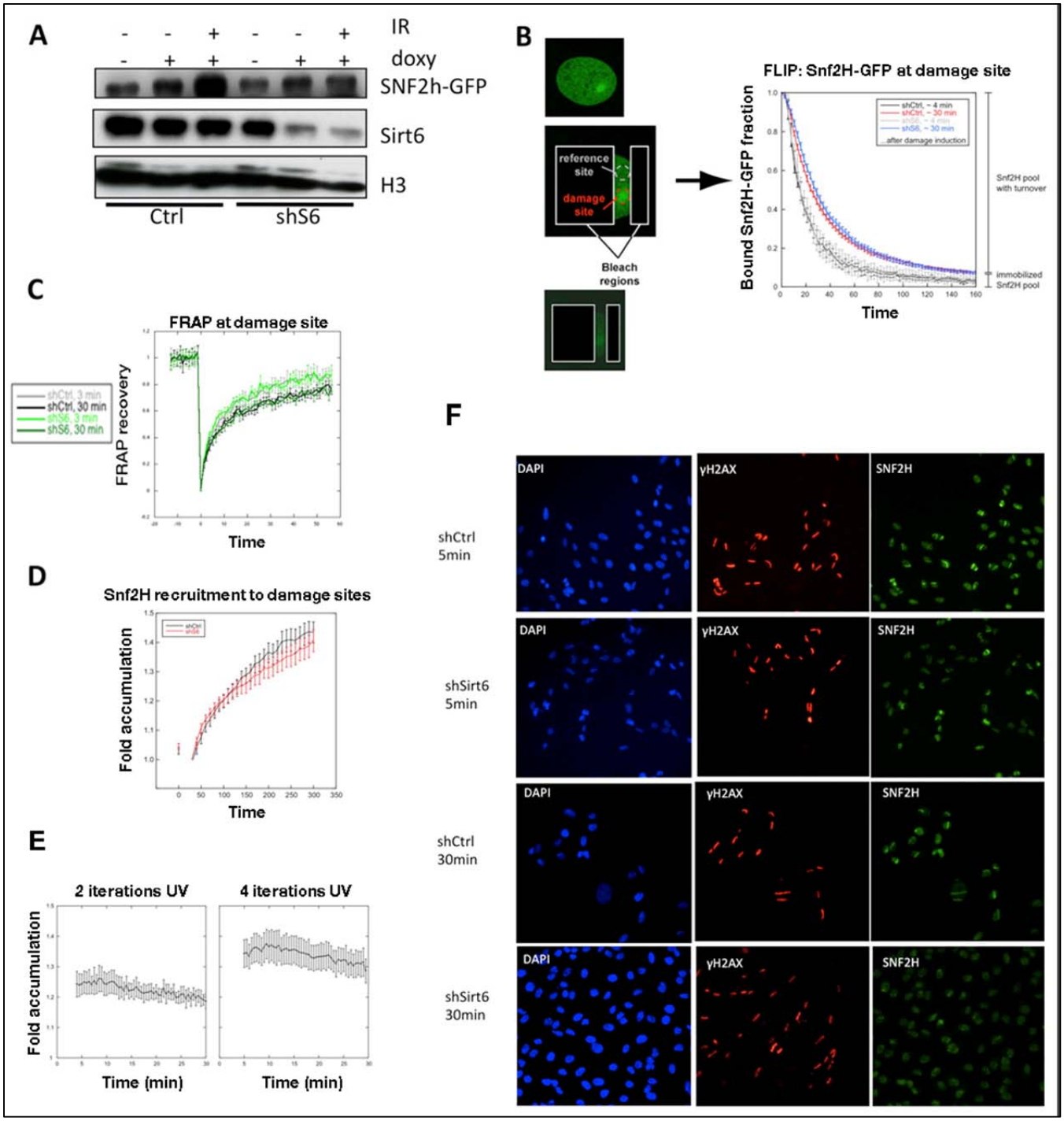
A
IR
doxy
SNF2h-GFP
Sirt6
H3
Ctrl
shS6
B
reference site
damage site
Bleach regions
FLIP: Snf2H-GFP at damage site
Bound Snf2H-GFP fraction
Time
Snf2H pool with turnover
immobilized Snf2H pool
C
FRAP at damage site
shCtrl, 3 min
shCtrl, 30 min
shS6, 3 min
shS6, 30 min
FRAP recovery
Time
D
Snf2H recruitment to damage sites
Fold accumulation
Time
E
2 iterations UV
4 iterations UV
Fold accumulation
Time (min)
Time (min)
F
DAPI
γH2AX
SNF2H
shCtrl 5min
shSirt6 5min
shCtrl 30min
shSirt6 30min

Figure S3. Related to Figure 3

A) Silencing of SIRT6 in U2OS-SNF2H-GFP cells shows effective silencing and less SNF2H-GFP in chromatin (note that doxycycline increases SNF2H levels in both cell lines, but SNF2H accumulation upon damage is impaired in the absence of SIRT6). B) FLIP results showing the decay in SNF2H-GFP taken from two time points, early (4min) and late (30 min) after irradiation. The adjacent areas of the cell are quenched to prevent measurement of the on-going accumulation of SNF2H-GFP. Fast decay occurs within the shCtrl and shSIRT6 in the early time points, while a slower decay is shown at later time points (indicative of rapid non-stable binding of SNF2H at early time-points). No difference is observed between shCtrl and shSIRT6 cells, indicating that SIRT6 is not stabilizing SNF2H at sites of damage by reducing its dissociation rate. C) Similar results were obtained when FRAP was performed to measure fluorescence recovery rather than fluorescence loss. D) Early recruitment (e.g. in non-presensitized/UV-only treated cells) of SNF2H shows no difference between shCtrl and shSIRT6 cells. E) Rapid decay of SNF2H in non-presensitized WT cells (mimicking oxidative damage). F) Examples of low-magnification pictures of immunostaining for the indicated proteins following laser-induced DNA damage. DAPI-stained nuclei are shown as staining control.

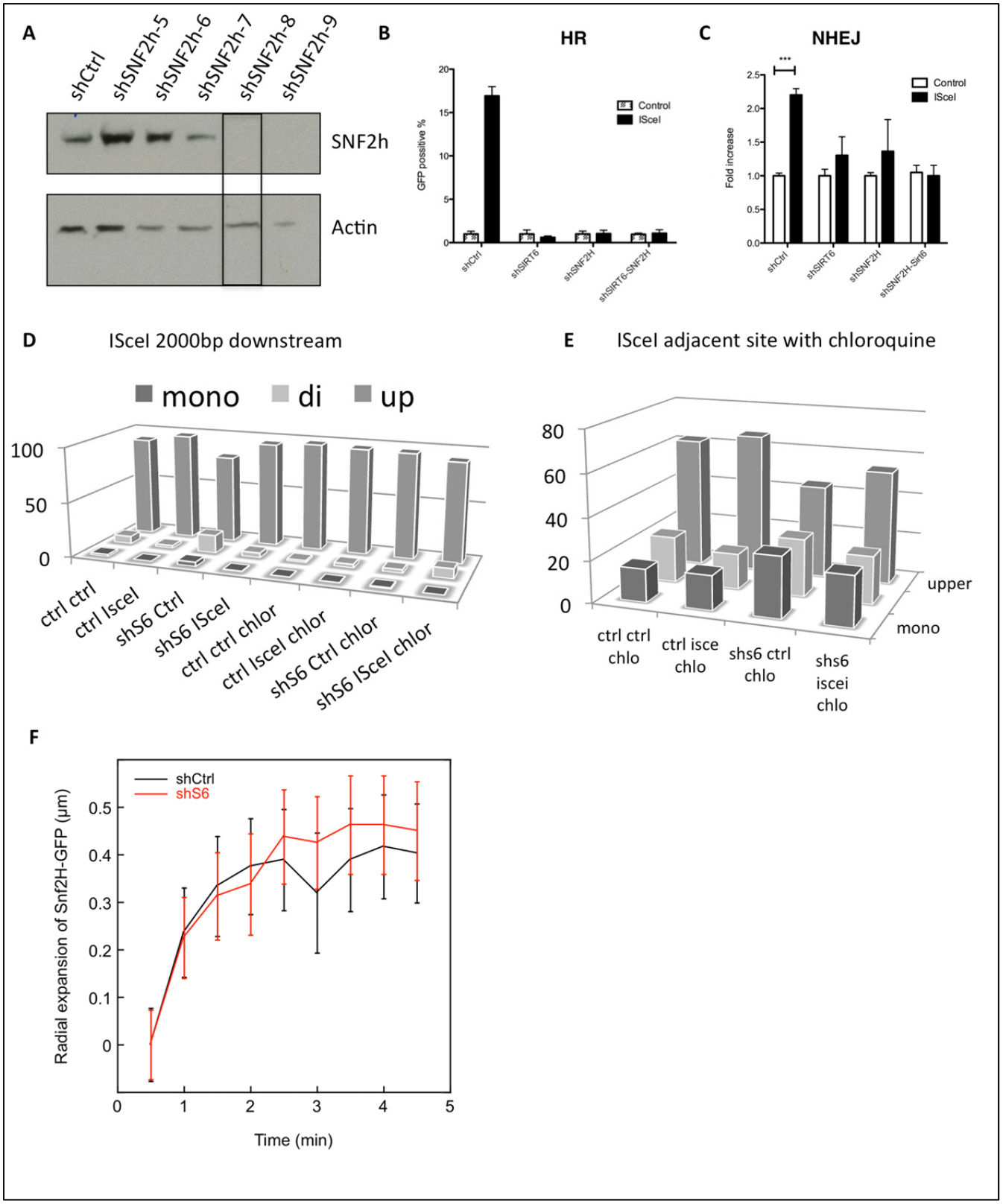
A
shCtrl
shSNF2h-5
shSNF2h-6
shSNF2h-7
shSNF2h-8
shSNF2h-9
SNF2h
Actin
B
HR
GFP possitive %
Control
ISceI
shCtrl
shSIRT6
shSNF2H
shSIRT6-SNF2H
C
NHEJ
***
Fold increase
Control
ISceI
shCtrl
shSIRT6
shSNF2H
shSNF2H-Sirt6
D
ISceI 2000bp downstream
mono
di
up
ctrl ctrl
ctrl ISceI
shS6 Ctrl
shS6 ISceI
ctrl ctrl chlor
ctrl ISceI chlor
shS6 Ctrl chlor
shS6 ISceI chlor
E
ISceI adjacent site with chloroquine
upper
mono
ctrl ctrl chlo
ctrl isce chlo
shs6 ctrl chlo
shs6 iscei chlo
F
shCtrl
shS6
Radial expansion of Snf2H-GFP (µm)
Time (min)

Figure S4. Related to Figure 4

A. 293T and U2OS cells were infected with 5 different shSNF2H hairpin sequences. We chose shSNF2H-8 for further experiments. **B, C.** shCtrl, shSIRT6, shSNF2H or shSNF2H-SIRT6 U2OS cells were co-transfected with DR-GFP (HR assay) or NHEJ-GFP plasmids and the I-SceI endonuclease or empty vector. Cells were analyzed by FACS at 72 hr for GFP presence, data is represented as mean +/- SEM. **D.** A region located 2Kb downstream of the I-SceI site shows no difference between shCtrl and shSIRT6 cells, with most of the chromatin in an inaccessible configuration (DNA mainly amplifies at the oligonucleosomes fractions). **E.** Chloroquine pre-treatment rescued the nucleosome-opening pattern, showing mono-nucleosomes, di-nucleosomes and upper (oligonucleosomes) to be more open and similar between WT and SIRT6-KD cells, data is represented as mean. **F.** Radial intensity profiles of Snf2H-GFP around the center of the laser-induced damage spot were calculated for different time points, their full width at half maximum (FWHM) was determined, and the difference to the initial FWHM was plotted. The size of the SNF2H-GFP bound region increased moderately and reached a plateau within 5 minutes after damage induction. No significant differences were observed between shCtrl and shSIRT6 cells. Error bars are +/- SEM.

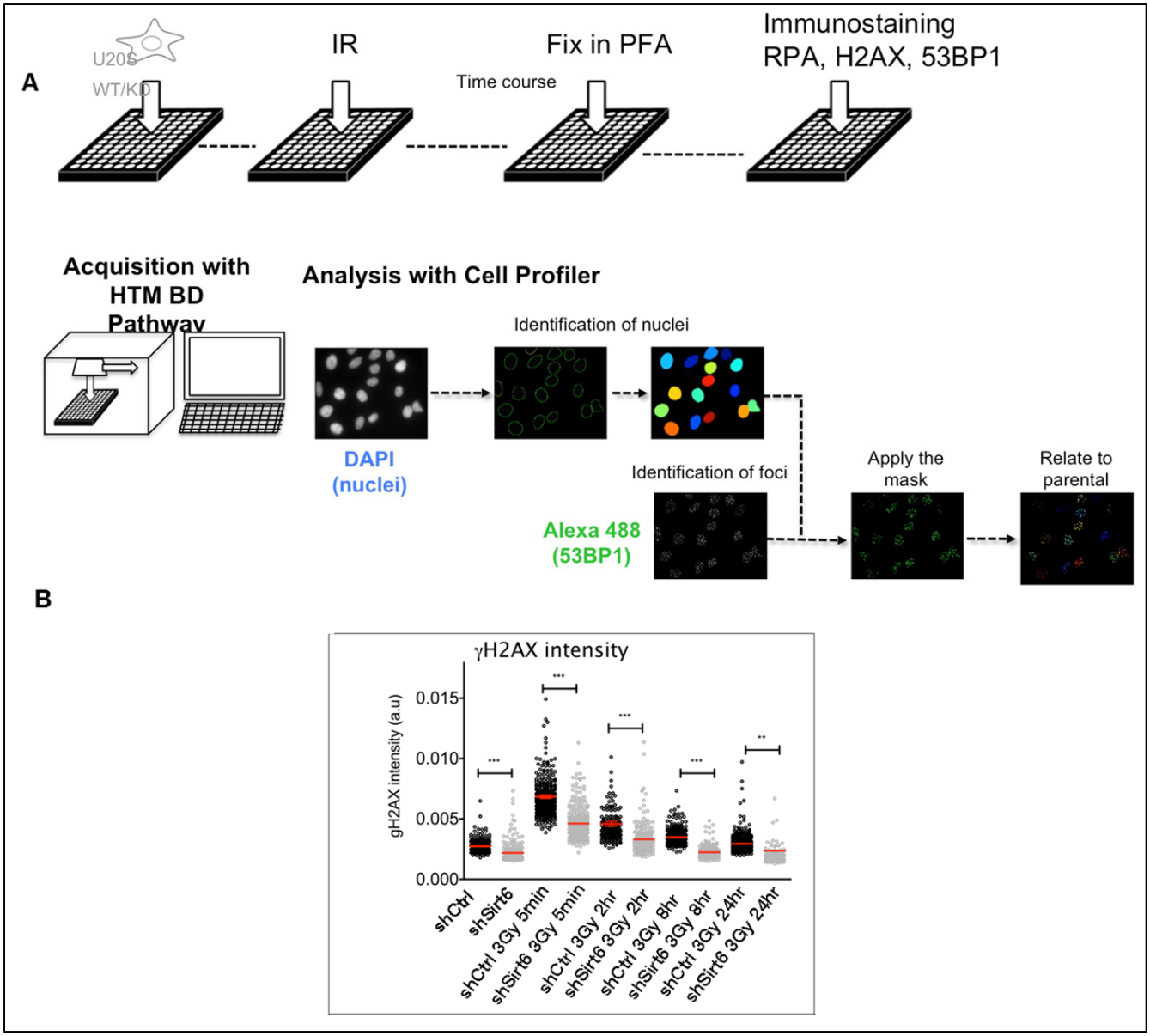

Figure S5. Related to Figure 5

A. Schematic representation of high-throughput microscope analysis. Cells were plated in 96 well plates, grown for 24 hr, and irradiated with 5Gy. Cells were fixed at different time points and immunostained with the indicated antibodies. 16 pictures per well were acquired, and three to six wells per treatment per experiment were used in two replicate experiments. Pictures were analyzed with the Cell Profiler Software by first recognizing the nuclei in each cell by DAPI staining, then analyzing the different channels (Alexa 555 for RPA or Alexa 488 for 53BP1), to identify foci number. Next, the software associates foci to each nucleus, giving foci number/cell. **B.** High-throughput analysis of γ-H2AX foci intensity following DNA damage, analyzed at indicated time-points in sh-Ctrl and sh-SIRT6 U2OS cells, data is represented as mean +/- SEM.

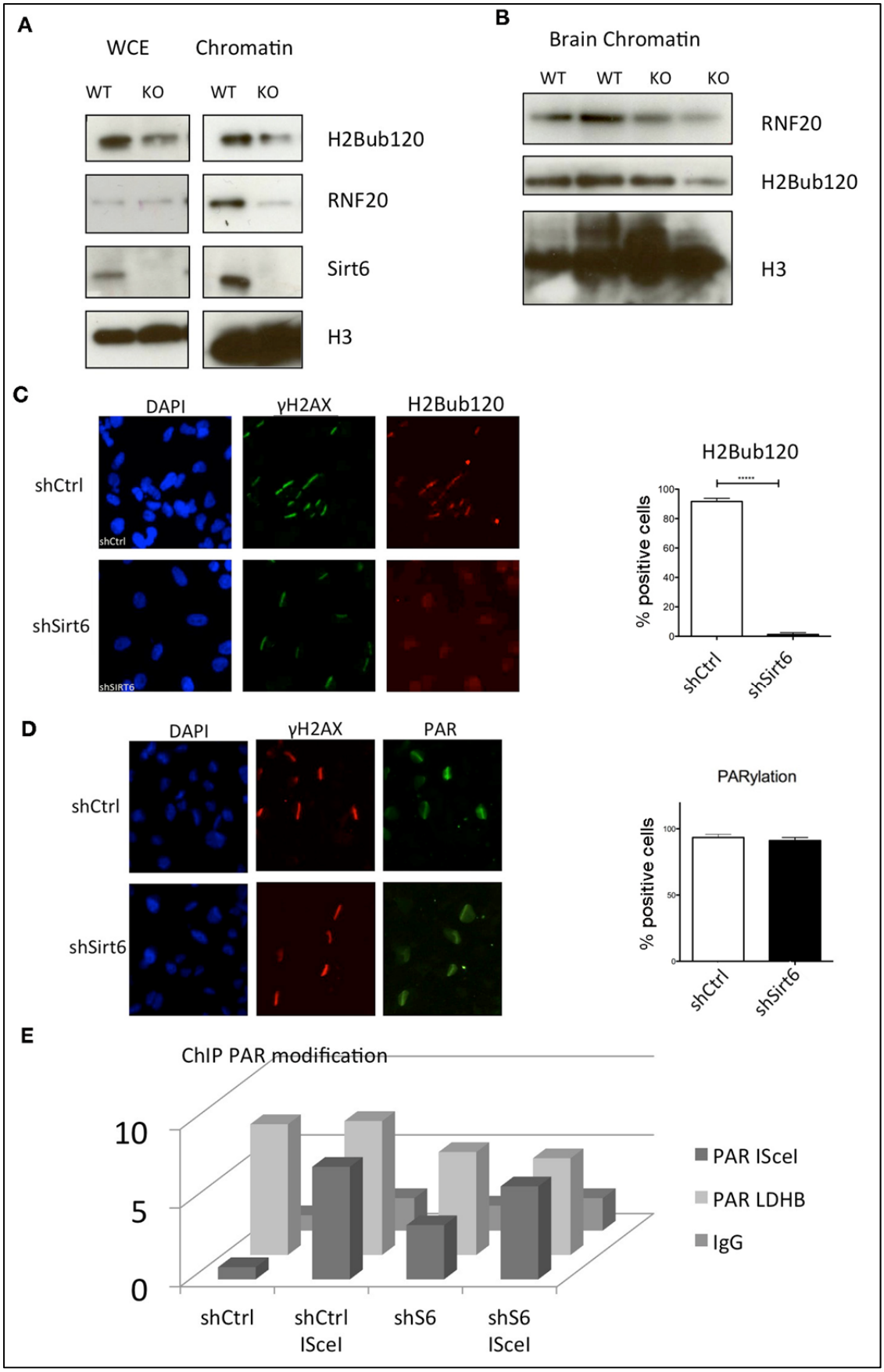
A
WCE
Chromatin
WT
KO
WT
KO
H2Bub120
RNF20
Sirt6
H3
B
Brain Chromatin
WT
WT
KO
KO
RNF20
H2Bub120
H3
C
DAPI
γH2AX
H2Bub120
shCtrl
shSirt6
shCtrl
shSIRT6
H2Bub120
% positive cells
100
80
60
40
20
0
shCtrl
shSirt6
D
DAPI
γH2AX
PAR
shCtrl
shSirt6
PARylation
% positive cells
100
50
0
shCtrl
shSirt6
E
ChIP PAR modification
10
5
0
shCtrl
shCtrl ISceI
shS6
shS6 ISceI
PAR ISceI
PAR LDHB
IgG

Figure S6. Related to Figure 6

A. Western blots with whole cell extracts and Chromatin extracts from WT or KO ES cells showing reduced levels of RNF20 in SIRT6 KO chromatin **B.** Western blot with chromatin extracts from brain of 22-days old SIRT6 WT and KO mice. **C.** Laser induced damage and immunofluorescece for H2Bub120 in shCtrl or shSIRT6 U2OS cells, data is represented as mean +/- SEM. **D.** Laser induced damage and immunofluorescece for PAR in shCtrl or shSIRT6 U2OS cells, data is represented as mean +/- SEM. **E.** ChIP of PAR modification in the I-SceI system shows a clear increase upon DNA DSB induction in both shCtrl and shSIRT6 cells indicating that SIRT6 is not influencing PARP1 activity in this system. The LDHB gene, a transcriptional target of SIRT6, shows no changes on PAR ChIP upon I-SceI induction.

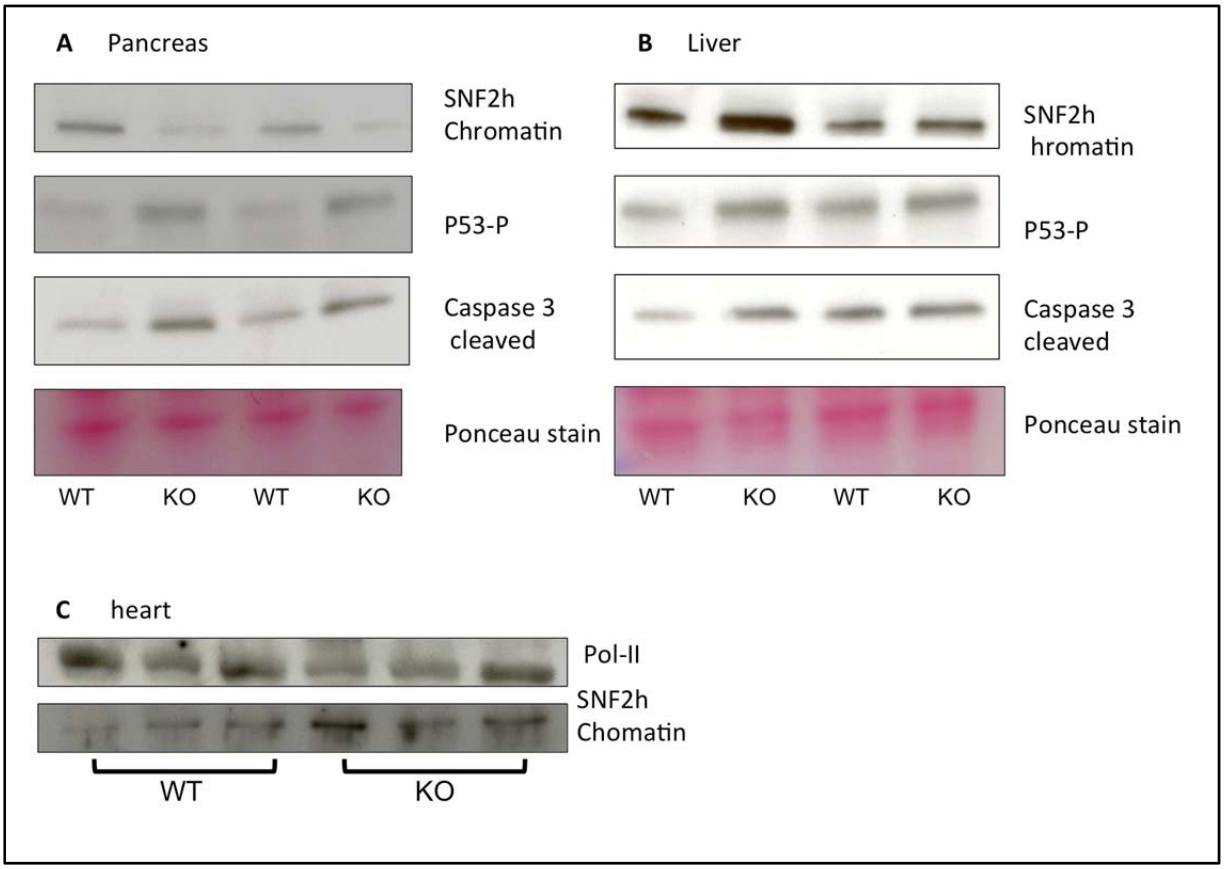

Figure S7. Related to Figure 7

A-C. Tissues from SIRT6 WT and KO mice were collected, and chromatin fractions were extracted. **A.** Pancreas shows a decrease of SNF2H in chromatin with concomitant increase in Caspase 3 cleavage and p53 phosphorylation . **B and C**. Liver and heart do not show defects in SNF2H recruitment, neither in activation of p53 or cleavage of Caspase 3.

Supplemental Experimental Procedures

Mass Spectrometry Analysis

Nuclear extracts were incubated overnight at 4°C with 2 ml of anti-FLAG M2 beads. Beads were washed 4 times with nuclear lysis buffer containing 100 Units of Micrococcal Nuclease (cat#10107921001, Roche) at 4°C. Bound proteins were eluted with FLAG-peptide (1mg/ml) and analyzed by immunoblotting. FLAG-purified material was separated using 4–20% gradient SDS–polyacrylamide-gel electrophoresis (SDS–PAGE) and stained with Silver Staining. Three gel slices (harboring 10-40Kda, 40-70Kda and 70kDa-up) were excised and analyzed by mass spectrometry at the Harvard Medical School Taplin Biological Mass Spectrometry Facility. Peptide selection was performed using an Xcorr cutoff > 2-3 and a ΔCn >0.08 in order to achieve an overall false positive rate of <1% as described (Peng et al., 2003). Mass spectrometry analysis revealed more than 300 proteins. From those who passed the threshold, SNF2H was among the top 5 enriched candidates, with numerous peptides covering ~80% of the protein identified in at least two replicates.

Western Blots and Immunostaining

Western blot analysis was carried out as previously described (Cheng et al., 2003).
The antibodies used in this study were as follows:
anti-SIRT6 (abcam) (WB 1:1000; IP and ChIP: 5µl for 1mg protein)
anti-SNF2H (NOVUS) (WB 1:1000; IF 1:500, IP and ChIP: 5ul for 1mg protein)
anti-H3K56Ac (Epitomics) (WB 1:1000, IF 1:500; IP and ChIP: 5ul for 1mg protein)
anti-Cleaved Caspase-3 (Abcam) (WB 1:1000)
anti-Cleaved PARP (Abcam) (WB 1:1000)
anti-P53-phospho (WB 1:1000)
anti-Flag (Sigma) (WB 1:3000; IP and ChIP: 5µl for 1mg protein)
anti-WSTF (Abcam) (WB 1:1000; IP and ChIP: 5µl for 1mg protein)
anti-ACF1 (Abcam) (WB 1:1000; IP and ChIP: 5µl for 1mg protein)
anti-SMC1 (NOVUS) (WB 1:1000)
anti-γH2AX (Millipore) (WB 1:1000; IF 1:500 brain culture; IF 1:2000 U20S)
anti-Tubulin (Sigma) (WB 1:1000)
anti H3 (Abcam) (WB 1:1000)
anti-53BP1 (NOVUS) (WB 1:3000; IF 1:500 brain culture; IF 1:2000 U20S)
anti-RPA32/34 (Abcam).

ChIPs and Quantitative RT-PCR

ChIP and qRT-PCR were performed as previously described (Zhong et al., 2010).
Primers used in this study:
myc-I-SceI down + AAGGGGAGTGGTTCAGGATT
myc-I-SceI down - ACGGAGTCGTAGTCGAGGTC
myc-I-SceI down2000 + GGACTATCCAGCTGCCAAGA
myc-I-SceI down2000 - AATTCAGGGATCTGGTCACG
DRGFP set 3R: TTGTAGTTGTACTCCAGCTTGTGC
DRGFP set 3F: TCTTCTTCAAGGACGACGGCAACT

ChIP-ReChIP

293T cells were co-transfected with CMV empty vector or Flag-SIRT6; and IsceI or empty vector together with the DR-GFP vector. 24hrs post transfection cells were washed with PBS and fixed in 1% Formaldehyde for 10 min at RT then Glycine for 5 min RT. Cells were washed with cold PBS three times and collected. Cell pellets were re-suspended in 10ml Lysis buffer-1 (*50 mM Hepes-KOH (pH 7.5), 140 mM NaCl, 1 mM EDTA, 10% Glycerol, 0.5% NP-40, 0.25% Triton X-100; freshly add protease inhibitors and PMSF*) and rocked for 10 min at 4C. Cells were spun down by centrifuge 1000g 4C and resuspended in Lysis Buffer-2 (*10 mM Tris-HCl (pH 8), 200 mM NaCl, 1 mM EDTA, 0.5 mM EGTA; freshly add protease inhibitors and PMSF*) rocking for 10 min at RT. After spinning pellets were resuspended in ChIP Lysis Buffer (*1% SDS, 10mM EDTA, 50mM Tris-HCl, pH 8*), and incubated for 30 min 4C on rotator. Samples were sonicated as previously described, and spun at 12000 rpm 4C, 15 min. Supernatant was collected and protein concentration was measured to compare between different samples. Same amount of protein was used for each ChIP. M2 sigma Flag beads were pre incubated with Antibody Binding Buffer (*PBS + 0.5% BSA, 1 mM PMSF, 0.02% Azide and Salomon Sperm*) O/N 4C rotating and washed 3 times and diluted in ChIP Dilution Buffer (*0.01% SDS, 1.1% Triton X-100,1.2mM EDTA, 16.7mM Tris-HCl, pH 8, 167mM NaCl*). ChIP lysates were diluted 1:10 in ChIP Dilution Buffer and incubated with the M2-Flag beads O/N on rotator in cold room. Next beads were washed at 4C, incubating on ice ~ 2 - 3 min between washes in the following order : 2x wash Low Salt (0*.1% SDS, 1%Triton X-100, 2mM EDTA, 20mM Tris-HCl, pH 8, 150mM NaCl*) 2x wash High Salt (*0.1% SDS, 1%Triton X-100, 2mM EDTA, 20mM Tris-HCl, pH 8, 500mM NaCl*) 2x wash LiCl Buffer (*0.25M LiCl,1% NP40, 1% deoxycholate, 1mM EDTA, 10mM Tris-HCl, pH 8.*) and 2x wash Low Salt Buffer. Beads were resuspend in 250 uL Low Salt Buffer supplemented with FLAG peptide to 0.2 mg/ml and Tris pH 8 to 200 mM. Incubated in rotation for 1 h 4C and sup collected (repeated 3 times) and the elutions were pooled. 75ul were kept to measure efficiency of the first ChIP and the second ChIP was performed using 325 of the eluted fraction of FLAG-SIRT6 ChIPs for SNF2H antibody and 325 ul for IgG using the previously described protocol.

MNase Assay-qPCR

$2x10^6$ shControl or shSIRT6 U2OS cells were transfected with a plasmid carrying the Isce-I site (ISce-I-pBSK, a kind gift from F. Alt (Wang et al., 2009). 48 h. later, cells with or without the Isce-I enzyme were homogenized with a Dounce homogenizer in RSB Buffer (10mM Tris-HCl pH 7.4, 10mM NaCl, 3mM $MgCl_2$, 0.5% NP-40, 1mM PMSF, 1mM DTT, Protease inhibitors). Cells were incubated on ice for 15 min and nuclei were collected by centrifugation (1000g), 10 min, 4°C, washed twice with RSB Buffer and digested with MNase in Digestion Buffer at room temperature (RT) (140 units, time course from 5-20 minutes). Reaction was stopped adding 1 volume of Stop Solution (50mM Tris-HCl pH 7.5,150mM NaCl, 50mM EDTA, 0.3% SDS). Samples were centrifuged at 10,000g for 10min at 4°C. DNA was purified by phenol-chloroform extraction and resolved in a 2% agarose gel. Bands were isolated and purified using a Gel Extraction Kit (Qiagen). Extracted DNA was used in q-PCR reactions as indicated.

Retroviral Infection

The RNAi Consortium hairpin plasmid clones for lentiviral expression of shRNA targeting SNF2H were described in (Moffat et al., 2006) and obtained from the Molecular Profiling Laboratory of the Massachusetts General Hospital Center for Cancer Research. The RNAi Consortium ID numbers of the hairpin clones are TRCN0000084430 and TRCN0000084431. SIRT6 WT and SIRT6 KO ES cells were infected by incubating with virus and 10mg/ml polybrene. Forty-eight hours later, cells

were selected in 2.5 μg/ml puromycin. From 5 different sequences 2 were selected for further work.

Plasmids

GST plasmids were generated by PCR, with the following SIRT6 primers:
N-terminus F-ATGTCGGTGAATTAT, N-terminus R- GGTGGTGTCAAACT, Core F-TTCGAGAATGCTCG, Core R-GGTGACAGACAGGTCTGC, C-Terminus F-CTGGGTACCTCGCTGCA, C-Terminus R-TCAGCTGGGGGCAGC Full length was generated with the forward N terminal and Reverse N terminal primers. The obtained fragments were cloned into the pGEX vector to generate a fusion protein containing the Glutathione S-Transferase (GST)-SIRT6 fragments.
SIRT6-Flag fragments ΔN, ΔC and Core were a kind present from Katrin Chua.
SIRT6-Flag and HY-SIRT6 flag were described previously (Zhong et al., 2010).

Homologous Recombination and Nonhomologous End-Joining Assays

We used a previously described (Pierce et al., 2001) U2OS cell line containing an HR reporter (U2OS-DR-GFP), a kind gift from P. Oberdoerffer. U2OS-DR-GFP cells were transfected with a tamoxifen-inducible I-SceI expressing vector (Promega). 24 h. later, I-SceI translocation to the nucleus was induced with Tamoxifen (200nM) for 24-48 h. Cells were collected and subjected to FACS analysis to determine percentage of GFP positive cells. For the double knockdown experiments, U2OS cells were transiently co-transfected with either DR-GFP (Pierce et al., 2001) for HR, or a GFP-NHEJ reporter (Seluanov et al., 2004), a kind gift of Michele Cea, and the Tamoxifen inducible I-SceI vector. Following 48-72h. Tamoxifen treatment, cells were collected and analyzed as previously indicated.

Generation of Histone-Mutant Plasmids

H3-Flag-HA was subcloned from the pOZ-H3.1-FH (kind gift from Dr. Yoshiiro Nakatani and Dr. Tsuyoshi Ikura) into the pBabe-puro using a PCR-based strategy. Briefly, H3.1-Flag-HA was amplified using a forward and a reverse primer including BamHI and SalI restriction sites, respectively (Fw: 5'-ggatcctgaaccatggctcgtacg-3'; Rv: 5'-gtcgacgccctaggcgtagtcggg-3') and cloned into the pBabe-puro. pBabe-H3.1-Flag-HA was used as a template to obtain the H3K56R and H3K56Q mutants by standard site-directed mutagenesis (primers used: 5'-cgtcgctaccagaggtccaccgagctg-3' and 5'-cagctcggtggacctctggtagcgacg-3').

High-Throughput Microscope

For quantification of 53BP1 and RPA foci, 16 pictures of each well were automatically acquired in a BD-Pathway 435 high-throughput microscope (Becton Dickinson) with AttoVision 1.5 software using a dry 40x magnification lens. Images were analyzed with Cell Profiler software. Briefly, images were segmented using the DAPI staining to generate masks matching cell nuclei. This mask was applied in the 53BP1 image to calculate the number of smaller objects (53BP1 foci) within larger objects (nuclei). 53BP1 foci were related to each parental nucleus allowing the determination of number of foci in each individual cell. All the images for quantitative analyses were acquired under non-saturating exposure conditions.

GST-SIRT6 Pull-Down of SNF2H

Assays were performed essentially as previously described (Mulligan et al., 2011). Briefly, pGEX4T1 plasmids containing full-length SIRT6, SIRT6 fragments 1-3, or empty vector control were

transformed into DE3pLysS E. coli and protein expression was induced overnight at room temperature in LB medium containing ampicillin (100 mg/mL), $ZnCl_2$ (10 mM) and IPTG (100 mM) (all from Sigma). Cells were then pelleted at 4000g for 15 min at 4°C and lysed in Buffer A (50 mM Tris (pH 8), 10% glycerol, 10 mM $ZnCl_2$, 1 mM PMSF (Sigma), 1 mM DTT (Sigma), 1X Complete EDTA-free Protease Inhibitors (Roche)) containing 0.5M NaCl (Sigma) and 1% NP-40 (Calbiochem). Lysates were centrifuged at 15,000g and supernatants incubated with glutathione Sepharose-4B beads (GE Healthcare) for 1 h. at 4°C. Beads were washed five times with Buffer A containing 1M NaCl and 1% NP-40, once with Buffer A containing 0.5M NaCl and 0.2% NP-40, and three times with Buffer A containing 140 mM NaCl and 0.05% NP-40. For binding assays, beads containing 2 ug of GST purified proteins were pre-incubated for 1h at 4°C in 250 µL Buffer A containing 20% Glycerol, 140 mM NaCl, 0.025% Bovine Serum Albumin (Sigma) and 0.05% NP-40. Purified recombinant SNF2H (~1µg) was then added, and beads incubated on a rotator for a further 3h at 4°C. Beads were then washed seven times with Buffer A containing 140 mM NaCl and 0.1% NP-40, proteins eluted in Laemmli Gel Loading Buffer at 95°C for 5 min., and analyzed by immunoblotting.

Real-Time Recruitment Kinetics to DNA Damage Sites

Cells were plated in a LabTek chamber 24 hours before the measurement. For presensitization, BrdU was added to the medium at a final concentration of 10 µM. For confocal imaging, a Leica SP5 microscope with a 63x oil immersion objective was used. Damage sites were induced by microirradiation with a UV diode laser at 405 nm and a power of 1.5 mW in the back aperture of the objective. After irradiation, either images were acquired every 10 seconds for 3 minutes within the same plane, or confocal image stacks were acquired every 30 seconds for 30 minutes. In the latter case, maximum intensity projections were used to correct for axial drift. Acquisition bleaching was normalized by calculating the ratio of the intensities within the irradiated region and within the whole cell nucleus.

Fluorescence Recovery after Photobleaching

Fluorescence recovery after photobleaching (FRAP) experiments were carried out using a Leica SP5 microscope with a 63X oil immersion objective. Images were acquired in 512 × 512 format with a scan speed of 1,400 Hz. Circular bleach spots with 2 µm diameter were used, which were positioned either at a damage site or at a distant reference site. Spots were bleached with an argon laser at 488 nm with a power of 1 mW in the back aperture of the objective. Acquisition bleaching was accounted for by normalizing the intensity in the bleach spot to the average intensity of the whole cell nucleus.

Fluorescence Loss in Photobleaching

For fluorescence loss in photobleaching (FLIP) experiments, damage sites were induced as described above and rectangular regions covering the nucleus adjacent to the damage site were continuously bleached, while the intensity within a small rectangular region around the damage site was recorded (see scheme in Supplementary Figure S3). For bleaching, an argon laser at 488 nm and a power of 1 mW in the back aperture of the objective was used. The intensity in the damaged region and in an adjacent reference region within the non-bleached part of the cell nucleus were quantified, and the intensity difference was plotted over time to obtain the mobile and immobile protein fractions.

Protein Expression and Purification
Flag-tagged SNF2H was purified as previously described (Bouazoune et al., 2009). SIRT6 was purified as noted in (Zhong et al., 2010).

Cell Culture Treatments
Puromycin resistant cells were selected with 2.5μg/ml puromycin, and maintained at 1ug/ml. Doxycycline inducible cells were treated with 1μg/ml of doxycycline and grown for as much as 4 weeks. Chloroquine (Sigma) concentration was 20μM.

Nucleosome Substrate Preparations
The DNA fragment used for nucleosome reconstitution was produced using the '601' strong nucleosome-positioning sequence (Lowary and Widom, 1998). The DNA was amplified by PCR and radiolabeled with a-^{32}P-dCTP. The DNA construct was purified using the QIAEX II® resin purification kit (Qiagen) according to the manufacturer's instruction. DNA was assembled into mononucleosomes by standard salt dialysis using histones purified from HeLa cells. The nucleosome assembly was purified over 10%–30% glycerol gradient before use.

Nucleosome Electrophoretic Mobility Shift Assay
Nucleosomes were assembled using 601 DNA core sequence +50-bp and histones purified from HeLa cells. The nucleosome EMSAs were carried out using a final concentration of 75 nM of nucleosomes (10 μL of nucleosomes in 12 mM HEPES pH 7.9, 10 mM TRIS pH 8.0, 50 mM NaCl, 4 mM $MgCl_2$, ~6% glycerol, 0.02% IGEPAL® CA-630 (Sigma-Aldrich), 0.15 mM EDTA pH 8.0) were mixed with 10 μL of protein(s) diluted in SDAC buffer (50 mM tris-Hcl pH 9, 4 mM $MgCl_2$, 50 mM NaCl, 0.5 mM DTT) to obtain the following final protein concentrations. Increasing concentrations of SIRT6 only (0.75, 1.5, 3 or 6 μM, lanes 2-5 respectively), increasing concentrations of SNF2H only (16, 32, 64 or 128 nM, lanes 6-9, respectively) or 1.5 μM SIRT6 (lane 10) in the presence of increasing concentrations of SNF2H (16, 32, 64 or 128 nM, lanes 11-14). After incubation on ice for 15 min, free and protein-bound nucleosomes were separated by 4.5% native PAGE, 0.5× TBE for about 2h30 at 110V, at 4˚C. Gels were stained with SYBR® Green according to the manufacturer's instructions. Data were quantified using the ImageJ software (NIH).

Comet Assay
Cells were irradiated (5Gy) and led to recover for the indicated times. 6 μl of cell suspension (6000 cells/μl) was then resuspended in 60 μl of 0.5% of low melting point agarose and led to solidify on clear slides precoated with 1% of normal agarose at 4°C. After solidification, the slides were placed in lysis solution (100 mM EDTA, 2.5 M NaCl, 10mM Tris Base, 10% glycerol and 1% Triton X-100) for 1 h at 4°C. Slides were washed twice in 1X TBE for 5 minutes and electrophoresed in 1X TBE at 1 V/cm for 15 min. After electrophoresis, gels were washed twice with water for 10 min and once with 70% ethanol for 5 min. Slides were dried on a heat block at 37°C and comets were visualized by staining DNA with DAPI. At least 50 comets per slide were scored. Images were captured with a fluorescence microscope and tail length was quantified using the Comet Assay IV software from Perceptive.

Chromatin Extraction
Cells were collected and washed in PBS, and resuspended in 2-5 pellet volumes of lysis buffer (10mM HEPES pH 7.4, 10mM KCl, 0.05% NP-40 and protease, deacetylase and phosphatase inhibitors). Samples were incubated 20 min on ice, and centrifuged at 14,000 rpm at 4°C for 10 min.

The supernatants containing the cytoplasmic proteins were removed and kept in a separate tube. Cell pellets were resuspended with 2-5 volumes of 0.2N HCl and incubated 20 min on ice, then centrifuged at 14,000 rpm at 4°C for 10 min. Supernatants were kept and neutralized with an equal volume of 1M Tris-HCl pH 8.

Laser-Induced DNA Damage

The day before the assay, cells were plated in a BD-Falcon glass-bottom plate and maintained in DMEM media without Phenol Red (10% FBS + Pen/Strep). Cells were incubated at 37^0C, washed with PBS and kept in media without Phenol Red (10% FBS + Pen/Strep). Prior to irradiation, cells were treated for 30 min with Hoechst 10μg/ml (pre-sensitization) and then washed with PBS and kept in DMEM media without Phenol Red (10% FBS + Pen/Strep). Laser microirradiation to generate DNA DSBs in defined nuclear volumes was performed using a MMI CELLCUT system containing a UVA laser of 355 nm (Molecular Machines & Industries). Following irradiation, cells were fixed at the indicated time-points and processed for immunostaining as indicated. Cells were analyzed using ImageJ software, where cells positive for γH2AX, were counted and analyzed to determine positivity for the different antibodies indicated in the manuscript. For each experiment, at least three independent repeats were performed, where an average of ~120 cells were analyzed per genotype. Student's t-Test was used to verify statistical significance.

Immunostaining

Cells were grown on coverslips covered with poly-L ornithine (Sigma) or grown directly in 96-well clear bottom plates (BD Falcon, cat no 353219) that were pretreated with 0.2 % gelatin. The next day, cells were irradiated with 3Gy and fixed at different time points and processed for immunofluorescence.

Two different permeabilization protocols were used: Doxycycline-inducible RFP cells were permeabilized with 100mM NaCl, 300mM Sucrose, 3mM MgCl2 and 10mM PIPES (pH 6.8) for 5 minutes at RT, then washed with PBS and fixed with 4% Paraformaldehyde 20min RT. Non-inducible cell lines were washed with PBS and fixed as noted. The protocol for both cell lines continues as follows: two washes with PBS 5 min RT, followed by permeabilization with 0.1% Triton X-100 in PBS as described (Bassing et al., 2002), 1hr blocking (0.3% BSA, 10% goat serum) and overnight primary antibody incubation at 4°C. Secondary antibodies used were Alexa 555 anti-mouse or 488 anti-rabbit (Roche).

Supplemental References

Bouazoune, K., Miranda, T.B., Jones, P.A., and Kingston, R.E. (2009). Analysis of individual remodeled nucleosomes reveals decreased histone-DNA contacts created by hSWI/SNF. Nucl. Acids Res. *37*, 5279-5294.

Cheng, H.L., Mostoslavsky, R., Saito, S., Manis, J.P., Gu, Y., Patel, P., Bronson, R., Appella, E., Alt, F.W., and Chua, K.F. (2003). Developmental defects and p53 hyperacetylation in Sir2 homolog (SIRT1)-deficient mice. Proc. Nat. Acad. Sci. USA *100*, 10794-10799.

Lowary, P.T., and Widom, J. (1998). New DNA sequence rules for high affinity binding to histone octamer and sequence-directed nucleosome positioning. J. Mol. Biol. *276*, 19-42.

Moffat, J., Grueneberg, D.A., Yang, X., Kim, S.Y., Kloepfer, A.M., Hinkle, G., Piqani, B., Eisenhaure, T.M., Luo, B., Grenier, J.K.*, et al.* (2006). A lentiviral RNAi library for human and mouse genes applied to an arrayed viral high-content screen. Cell *124*, 1283-1298.

Mulligan, P., Yang, F., Di Stefano, L., Ji, J.Y., Ouyang, J., Nishikawa, J.L., Toiber, D., Kulkarni, M., Wang, Q., Najafi-Shoushtari, S.H.*, et al.* (2011). A SIRT1-LSD1 corepressor complex regulates Notch target gene expression and development. Mol. Cell *42*, 689-699.

Peng, J., Schwartz, D., Elias, J.E., Thoreen, C.C., Cheng, D., Marsischky, G., Roelofs, J., Finley, D., and Gygi, S.P. (2003). A proteomics approach to understanding protein ubiquitination. Nat. Biot. *21*, 921-926.

Pierce, A.J., Hu, P., Han, M., Ellis, N., and Jasin, M. (2001). Ku DNA end-binding protein modulates homologous repair of double-strand breaks in mammalian cells. Genes & Dev. *15*, 3237-3242.

Seluanov, A., Mittelman, D., Pereira-Smith, O.M., Wilson, J.H., and Gorbunova, V. (2004). DNA end joining becomes less efficient and more error-prone during cellular senescence. Proc. Nat. Acad. Sci. USA *101*, 7624-7629.

Zhong, L., D'Urso, A., Toiber, D., Sebastian, C., Henry, R.E., Vadysirisack, D.D., Guimaraes, A., Marinelli, B., Wikstrom, J.D., Nir, T.*, et al.* (2010). The histone deacetylase Sirt6 regulates glucose homeostasis via Hif1alpha. Cell *140*, 280-293.